LOCALIZED MAGNETIC FLUID FINISHING OF FREEFORM SURFACES USING ELECTRO-PERMANENT MAGNETS AND MAGNETIC CONCENTRATION

A Thesis

by

ISKANDER EL AMRI

Submitted to the Office of Graduate and Professional Studies of
Texas A&M University
in partial fulfillment of the requirements for the degree of

MASTER OF SCIENCE

Chair of Committee,	Satish T.S. Bukkapatnam
Co-Chair of Committee,	Arun Srinivasa
Committee Member,	Dinakar Sagapuram
Head of Department,	Andreas Polycarpou

August 2018

Major Subject: Mechanical Engineering

ABSTRACT[1]

We report the implementation of a novel magnetic concertation setup for localized finishing of freeform surfaces based on employing electro-permanent magnet arrays configured using a recently developed magnetic concentration principle. The setup, without the use of any rotating or moving component, is capable of creating a localized spatiotemporal magnetic field variation in the specialized magnetic fluid to polish a target 1.5cm^2 area on the workpiece surface. Using a computational mechanistic model as well as experimental studies, we show that the current configuration of electro-permanent magnets is capable of amplifying the magnetic strength by almost 3 times near the workpiece surface in comparison to no magnetic concentration. We also show that by modulating the strength, including toggling the polarity of electro-permanent magnets, we demonstrate the sloshing motion of the fluid at a targeted region without requiring any rotating part.

A set of experiments was conducted to study the capabilities of the experimental setup. The first experimental investigation looked at the localized and selective removal of acrylic paint applied from a differential geometry. The second experimental study looked at improving the surface roughness of 3D printed polyurethane dogbone samples. The process was capable of reducing the SA values from 11 µm initially to .7 µm.

---

[1] Parts of the abstract are reprinted with permission from "Localized magnetic fluid finishing of freeform surfaces using electropermanent magnets and magnetic concentration" by Iskander El-Amri, Ashif Sikandar Iquebal, Arun Srinivasa, Satish Bukkapatnam, 2019. Journal of Manufacturing Processes,2018 https://doi.org/10.1016/j.jmapro.2018.05.026 , Copyright 2018 by Elsevier

DEDICATION

This work is dedicated to my family and friends who encouraged and helped me during my studies at Texas A&M University. Thanks for their constant support that made me go through the graduate program.

ACKNOWLEDGEMENTS

I would like to thank my committee chair, Dr. Satish Bukkapatnam, and my committee members, Dr. Arun Srinivasa and Dr. Dinakar Sagapuram, for their guidance and support throughout the course of this research.

Thanks also go to my friends and colleagues and the department faculty and staff for making my time at Texas A&M University a great experience.

Finally, thanks to my mother, father and my siblings for their encouragement and to my fiancée for her patience and love.

CONTRIBUTORS AND FUNDING SOURCES

Contributors

I would like to thank my graduate research advisor and committee chair Dr. Bukkapatnam, who provided exceptional environment for conducting a research in magnetic polishing. I would also like to thank my committee co-chair member, Dr Srinivassa and committee member Dr. Sagapuram for their guidance and support throughout my research. Special thanks to Ashif Sikandar Iquebal for helping with experiments and suggestions. All other work conducted for the thesis was completed by the student independently.

Funding Sources

Graduate study was supported by a graduate teaching assistant funding from Texas A&M University and a support from the National Science Foundation through grant CMMI- 1538501.

NOMENCLATURE

ALM	Additive Laser Manufacturing
AM	Additive Manufacturing
CMP	Chemical Mechanical Polishing
DF	Down Force
ERF	Electrorheological Fluid
FEM	Finite Element Method
FEMM	Finite Element Method Magnetics
MF	Magnetic Fluid
MRF	Magnetorheological Fluid
MRR	Material Removal Rate
P	Pressure
PWDM	Pulse Width Modulation
Sa	Surface Roughness
T	Time

TABLE OF CONTENTS

LIST OF FIGURES

LIST OF TABLES

1. INTRODUCTION[2]

1.1 Introduction

Recent advances in additive and hybrid manufacturing technologies have created several opportunities to manufacture complex, freeform components with differential surface morphology and microstructure to deliver enhanced performance [1]. The ability of AM technology to fabricate custom components with net near shape and enhanced functionalities has created a massive demand for additive manufactured parts, especially in automobile, aerospace and biomedical implant industry with an estimated market size of about $4 billion in 2017 and expected to surpass $13 billion by 2025 [2].

However, with increasing part complexity, challenges pertaining to that of surface quality and porosity has also increased. For example, biomedical implants (such as knee and hip implants) require specular surface finish ($S_a < 20$ nm) to promote wear mitigation at the joints and other the bearing surfaces. In contrast, a rough, textured surface is desired along the vast swathes of the part to promote osseointegration (i.e., direct structural and functional connection between ordered living bone and the surface of a load-carrying implant). In aerospace and automobile industry, post-processing of additive manufactured

---

[2] Parts of the introduction are reprinted with permission from "Localized magnetic fluid finishing of freeform surfaces using electropermanent magnets and magnetic concentration" by Iskander El-Amri, Ashif Sikandar Iquebal, Arun Srinivasa, Satish Bukkapatnam, 2019. Journal of Manufacturing Processes,2018 https://doi.org/10.1016/j.jmapro.2018.05.026 , Copyright 2018 by Elsevier

components, e.g., turbines and shafts—with hard-to-reach free-form geometries— require finished surfaces to allow undisrupted flow. However, conventional machining and finishing approaches are incapable of finishing hard-to-reach surfaces.

Realization of spatially specific texturing and finishing of such complex shapes and structures to meet the desired functionalities necessitate localized finishing and targeted modification of freeform surfaces. Conventionally, the industry employs manual hand-held polishers for localized finishing. Such processes tend to be laborious and demand extreme dexterity. Alternatively, localized electro-chemo-mechanical etching methods have been investigated, but they need some masks or physical barriers to confine material removal at desired locations. While localization is hard to achieve with free-abrasive methods, many geometric features are inaccessible to hand-held polishers.

Advancements in magnetic fluids and magnets design offer new opportunities [3]–[11] to create adaptable tools that combine the best features of conventional finishing tools (flexible downforce, localization) and the flexibility provided by fluids to reach tight spaces to enable a fast, automated and localized finishing of hard-to-access locations. Significant research exists on utilizing the abrasive-mixed magnetorheological fluid as a magnetic abrasive brush [1] to finish planar surfaces. Consequently, conventional magnetic polishers are limited to flat geometries or require the application of complex robotic arms or CNC machines to finish free-form surfaces using the magnetic abrasive brush. However, only limited research has focused on creating spatiotemporal variation in the magnetic fields that could be utilized to access these hard-to-access locations.

1.2 Research Motivation & Objective

With the rise of the additive manufacturing, engineers and scientist can create unique parts that combine intricate geometries with complex functionalities. However, the parts generated with the AM techniques cannot be directly used since they need to undergo many post-processing operations to eliminate the support structures and to improve the surface roughness. Traditionally, improving the surface toughness was done with handled tools that require skilled labor and a tremendous amount of time which will impact the cost of the part and induce variability in the quality of the product due to the human factor. However, thanks to the development in magnetorheological fluids and the advancement in electro-permanent magnet technology made it possible to create a flexible polishing tool that can remove material from interior surface/ complex surfaces relying only on the sharp changes in the magnetic field. To achieve this goal, the following research object must be addressed:

- Investigate and characterize various compositions of magnetic fluid blobs—that lend themselves to stiffen and agitate under suitable magnetic fields optimally
- Derive spatiotemporal magnetic field patterns best suited for local polishing (desired local down pressure and fluid flow pattern) via novel ray-tracing based path planning methods
- Specify the magnetic system (consisting of a suitably positioned electro-permanent magnet) to generate the desired spatiotemporal fields

2. LITERATURE REVIEW[3]

In this section, we present a comprehensive survey of the literature discussing the nonmagnetic localized polishing processes. Then, we are going to investigate the various efforts in the magnetic polishing process and cover the critical process parameters and underlying mechanics. We also review the recent works that have reported simulation efforts in localizing and concentrating the magnetic field lines at an arbitrary location away from the poles.

2.1 Localized Polishing

In this section, we present the traditional methods attempted to create a localized finishing and we divided these processes according to the material removal mechanisms in play.

2.1.1 Chemical Mechanical Methods: Chemical Mechanical Polishing

Chemical Mechanical Polishing (CMP) was first developed in 1963 by Robert J. Walsh et al. [12]. The process was used to create defect-free semiconductor wafers by combining a mechanical polishing action, provided by a rotary polishing disk pressing

[3] Parts of the literature review are reprinted with permission from "Localized magnetic fluid finishing of freeform surfaces using electropermanent magnets and magnetic concentration" by Iskander El-Amri, Ashif Sikandar Iquebal, Arun Srinivasa, Satish Bukkapatnam, 2019. Journal of Manufacturing Processes,2018 https://doi.org/10.1016/j.jmapro.2018.05.026 , Copyright 2018 by Elsevier

down on the surface of the wafer, and a chemical polishing action created by abrasive particles suspended in a slurry (see Fig. 1).

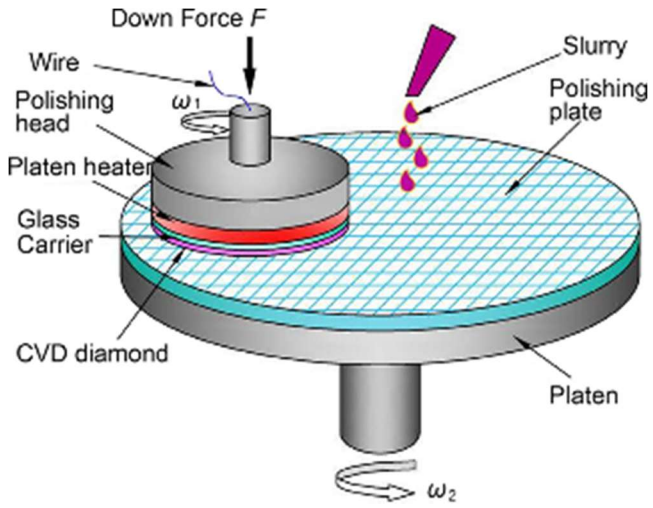

Figure 1: Chemical Mechanical Polishing Slurries for Chemically Vapor-Deposited Diamond Films (Reprinted from [53])

During CMP [13]–[16], the abrasive slurry is pumped at the pad/workpiece contact interface where the individual abrasive particles are moving in the same direction of the pad while also sliding and rolling against the target surface. This range of motion is known as a 3-body abrasion mechanism [17] (see Fig. 2) and is very useful in creating a fine finish surface with little scratch marks or surface defects.

CMP is typically utilized to create a uniform finish across a targeted surface and does not have the capability to address areas with high surface irregularities locally,

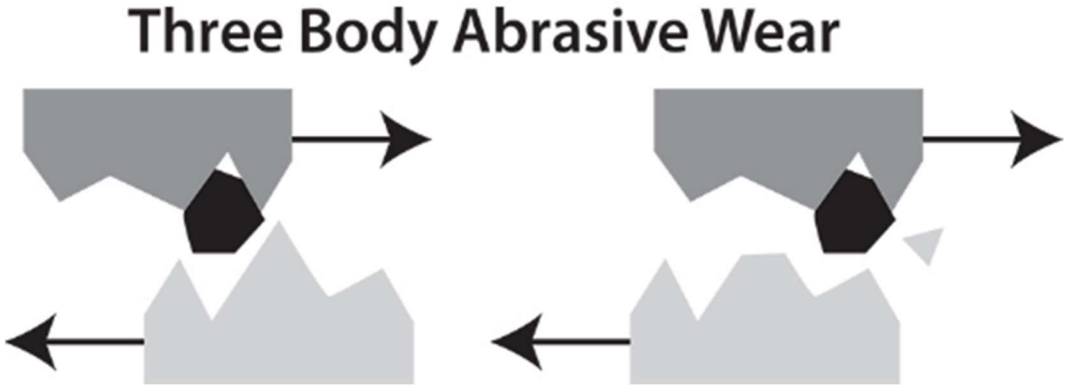

Figure 2: Schematic showing the motion of the abrasive particles in a three-body abrasion (Reprinted from [17])

however, new advancements in polishing pad designs and advanced surface roughness measuring devices have enabled the use of CMP in localized small areas.

For example, Yutaka et al. [18] developed a new CMP setup that utilizes a rotating polishing pad smaller than a fixed workpiece. The setup controls the oscillations patterns of the pad depending on the surface roughness values collected by a data collection system

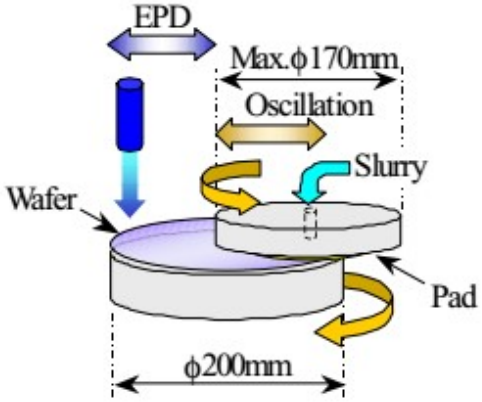

Figure 3: Schematic showing a CMP polishing process with pads smaller than workpiece designed for localized polishing (Reprinted from [18])

(see Fig. 3). Ring-shaped polishing pads[19] (Fig. 4) ; can also be used to focus the polishing action on a specific region of the target surface. However, this new setup requires in situ surface roughness measurement system and custom-made polishing pads which add to the cost of this method. Moreover, this method is only applicable for planar geometries which restricts the versatility of the process.

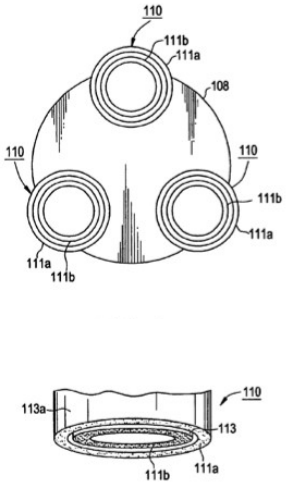

Figure 4: Schematic novel design of polishing rings utilized to create localized polishing (Reprinted from [19])

2.1.2 Energy Based Method: Laser Polishing

Laser beams have been utilized in polishing processes that were demonstrated to yield a very high-quality surface finish, especially of metallic parts. Three main strategies are exploited in this process including large area ablation, localized ablation and material re-melting [20] .

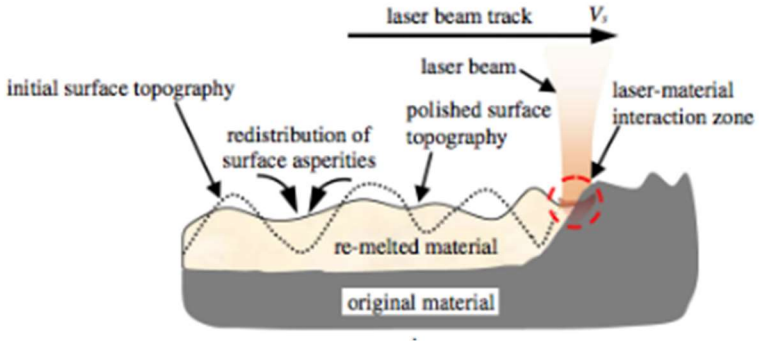

Figure 5: Schematic showing the surface profile of a workpiece during laser polishing (Reprinted from [20])

Recently, more efforts were focused on the laser re-melting technique (see Fig. 5) since it offers shorter cycle times, better control over the surface roughness in a localized area where the process can achieve a surface roughness of 5 nm (see Fig. 6). During this process, a laser beam melts the surface peaks which are then redistributed in adjacent valleys via capillary action resulting in the reduction of the peak to valley ratio thus creating a smoother surface. Combining the laser re-melting process with a CNC machine was proven effective in the polishing of freeform geometries[20]–[23].

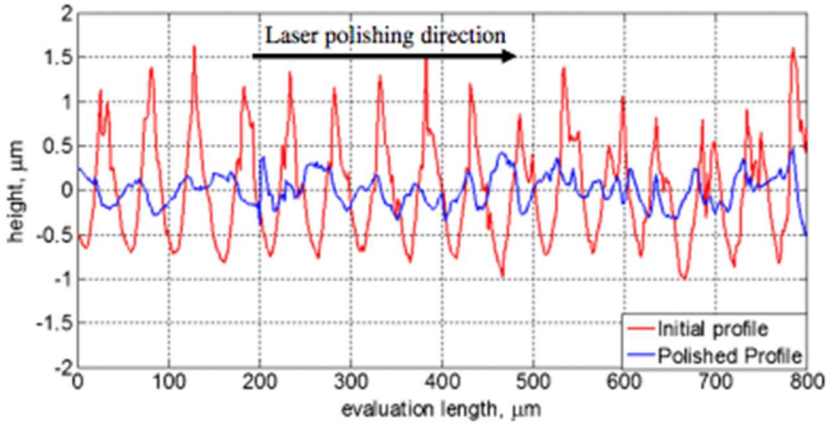

Figure 6: Surface profile of a workpiece before (red profile) and after polishing (blue profile) (Reprinted from [20])

Rosa et al. [23] have investigated using a polish as you print strategy where the same laser source used during the laser sintering process is also utilized to polish the newly printed areas. This method allows to finish the workpiece during the printing process, and it was demonstrated to polish interior surface and hard to reach areas. A multi-pass strategy was utilized where the laser beam was applied N times to the desired areas while keeping the same parameters.

This approach was capable of reducing the surface roughness of an ALM 316L printed from 21 µm to 0.79 µm a surface finish of 0.79 µm, thus a 96% improvement in surface roughness (see Fig. 7 & 8). However, this method requires a surface roughness measurement device to get an initial reading of the surface profile to target the peaks

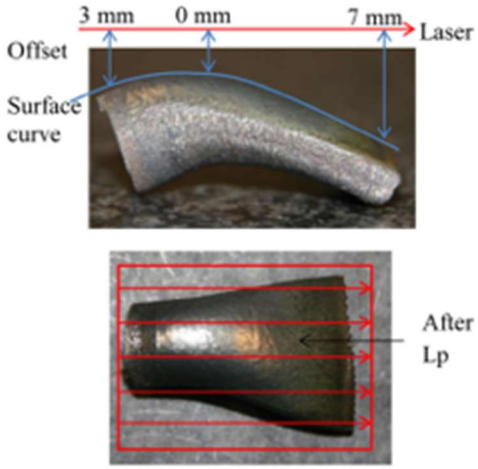

Figure 7: Photograph showing a complex part surface before and after laser polishing (Reprinted from [23])

exclusively in the desired location. It requires as well as a CNC program generated from a 3D model of the workpiece. Another drawback of this method is that it can create heat affected zones where the defects can propagate [20].

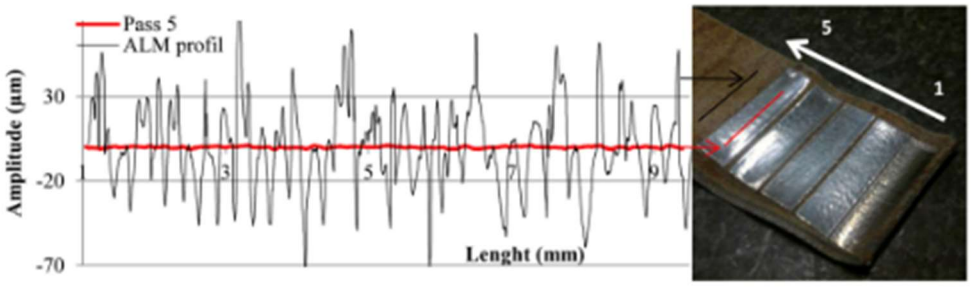

Figure 8: Schematic displaying the surface roughness improvement after five passed with the laser polishing process (Reprinted from [23])

2.1.3 Chemico-Electrical Methods

2.1.3.1 Electrochemical Polishing

Electrochemical polishing has been used to create high surface finish parts. The workpiece, anode here, is submerged in a bath of electrolyte where current is passing through. With the passage of current, material is removed from the anode and deposited on the cathode thus improving the surface roughness of the parts.

For example, Zhang et al. [24] have utilized electrochemical polishing to create 3D microstructures on a Si (100) workpiece (see Fig. 9) by using an agarose stamp which serves as a guide to localizing the material removal action in specific areas. Under vacuum, the micropattern guide is placed in a beaker filled with agarose gel which seeps into the smallest details of the stamp. The gel acts as current conductor thus allowing for a precise material removal following the stamp (see Fig. 9 & 10).

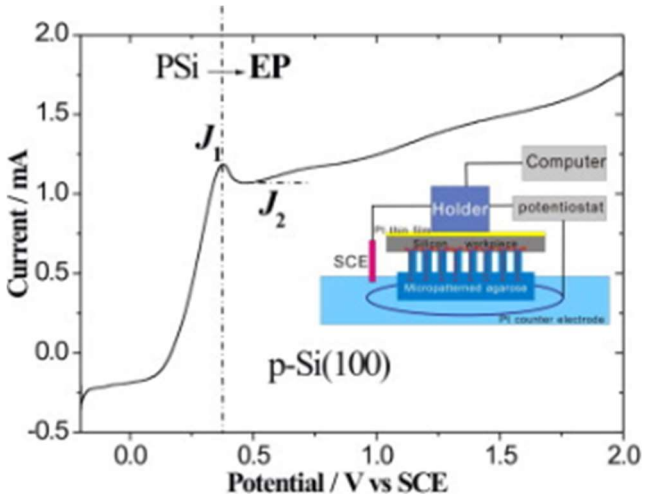

Figure 9: Schematic showing the localized electrochemical polishing setup (Reprinted from [24])

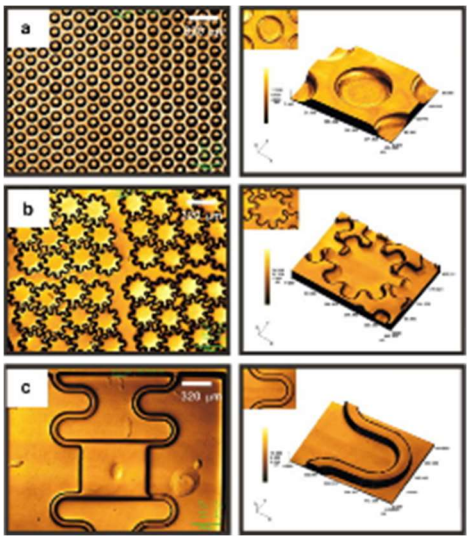

Figure 10: Photograph showing patterns generated by electrochemical polishing (Reprinted [24])

Researchers have tested with a pulsed current to polish microstructures machined on steel plates [25]. This method yielded better results in polishing localized features than other electrochemical polishing techniques (see Fig. 11). However, this technique only works with conductive materials and can create corrosion on the surface of the workpiece.

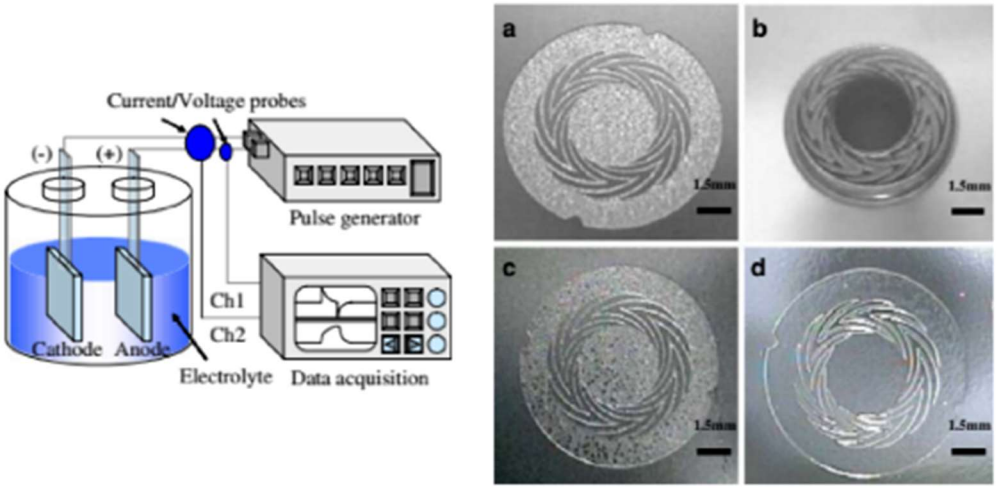

Figure 11: Schematic showing the electrochemical process and the resulting fine details on polished surface (Reprinted from [25])

2.1.3.2 Electrorheological Polishing

Electrorheological fluid (ERF) are fluids that are a combination of non-conductive particles suspended in an insulating liquid. When current is applied through the ERF, the viscosity of the suspension goes from low to a gel-like. This property has been utilized to polish microstructure because the fine abrasive particles suspended in the ERF become polarized when an electric current is passing through thus forming a collection of stable chains of particles [26]. As shown in figure 12, when the electrode encloses the polishing tool, electric field lines radiate from the tip of the tool, aligning the particles along these lines. By rotating tool, a polishing action is created underneath the target region.

Combining the tool with a surface profilometer (Fig. 12), this method enables to selectively polish asperities in target regions. However, this process is time-consuming since it has a low material removal rate and needs costly scanning equipment.

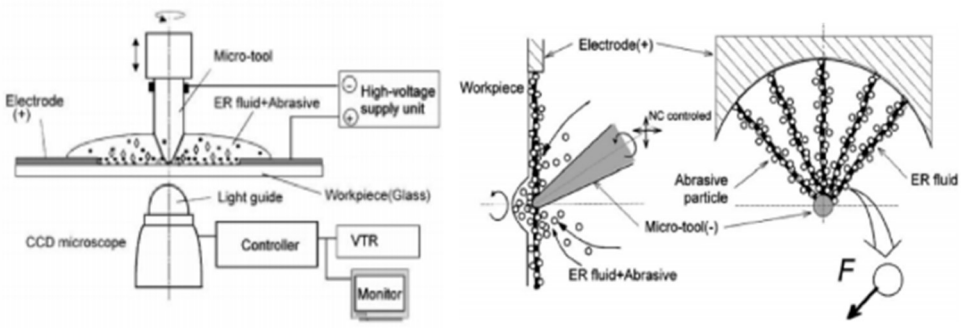

Figure 12: Schematic showing the components of the electrorheological polishing process and the material removal mechanism (Reprinted from [26])

2.1.4 Mechanical Methods

2.1.4.1 Bonnet Polishing

Bonnet polishing or “precession” is a technique that uses a flexible inflatable membrane which continually presses against the target surface [27]. The bonnet tool is rotated via a CNC machine to achieve polishing (see Fig. 13). The flexibility of Bonnet allows it to polish freeform shapes with a high level of localization. This process uses fine abrasive slurry in conjugation with the flexible tool to remove material. However, this method depends highly on the precision of the rotating machine and is also not able to polish the internal surface.

Figure 13: Photograph showing the Bonnet polishing flexible head mounted on CNC (Reprinted from [27])

To overcome the problems addressed in the previous section, some researchers proposed that magnetic polishing process be a possible polishing method for localized

freeform geometry finishing because magnetic slurry can form a flexible tool that can adapt to the surface profile of the workpiece. Recently, researchers have proposed many variations of the magnetic abrasive polishing technique, which we are going to discuss in this section.

2.2 Magnetic Polishing

2.2.1 Working Principles

During the magnetic polishing, the magnetic particles align themselves with the field lines to form chain-like structures which constitute the flexible magnetic brush. This brush applies two forces on the surface of the workpiece namely: a normal force (F_N) packs the magnetic abrasive particles against the surface of the workpiece and is also responsible for the micro indentations on the surface. The tangential force (F_T) is a result of the movement of the flexible magnetic brush and is responsible for the microchipping of the asperities of the workpiece surface [28].

The normal force F_N and tangential force F_T are transferred from the ferromagnetic particles close to the surface to the abrasive particles; thus, we can model the magnetic polishing process as a cutting process with a negative rake angle (see Fig. 14).

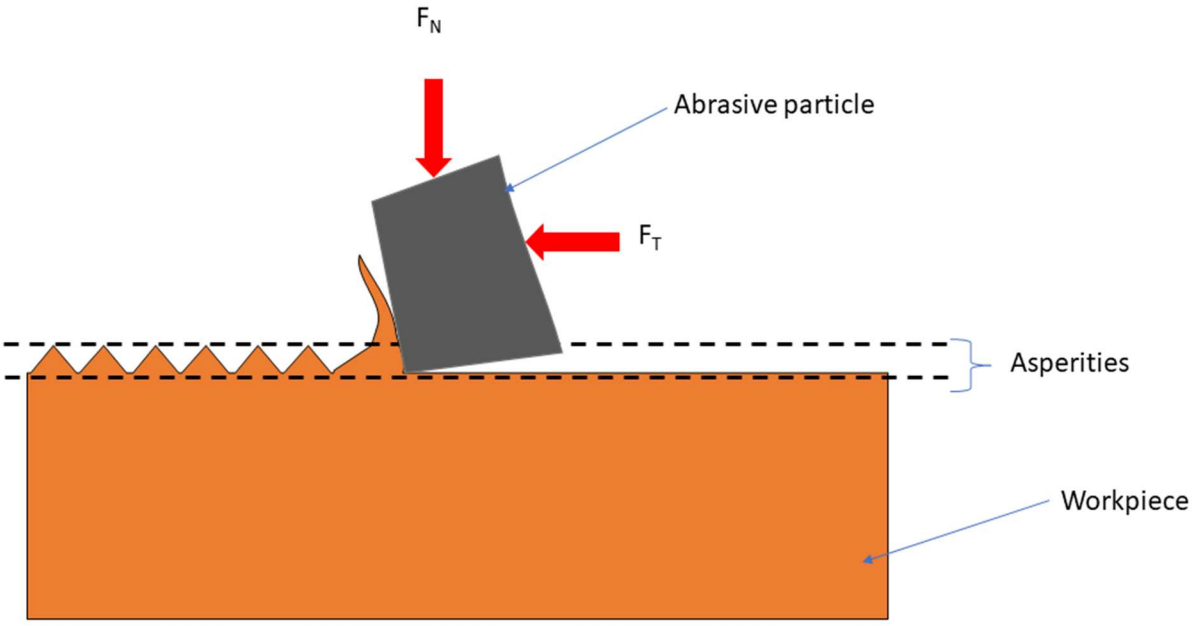

Figure 14: Schematic displaying the forces acting on an abrasive particle during the magnetic polishing process

For an arbitrary position, F_N and F_T can be expressed as the sum of two forces F_x along the direction of the magnetic force line and F_y along the magnetic equipotential lines F_x and F_y can be expressed by the following equations [28]:

$$F_x = \chi^s \, \mu_0 V H \left(\frac{dH}{dX}\right) \qquad \textbf{EQ 2-1}$$

$$F_y = \chi^s \, \mu_0 V H \left(\frac{dH}{dY}\right) \qquad \textbf{EQ 2-2}$$

where χ^s is the magnetic susceptibility of the magnetic particles $\frac{dH}{dX}$ and $\frac{dH}{dY}$ are the gradients of the magnetic field in the x and y directions respectively. From Fig. 15, we can express F_N and F_T in terms of F_x and F_y by using the following relation [28]:

$$F_N = F_x cos\theta - F_y sin\theta \quad \textbf{EQ 2-3}$$

$$F_T = -F_x sin\theta - F_y cos\theta \quad \textbf{EQ 2-4}$$

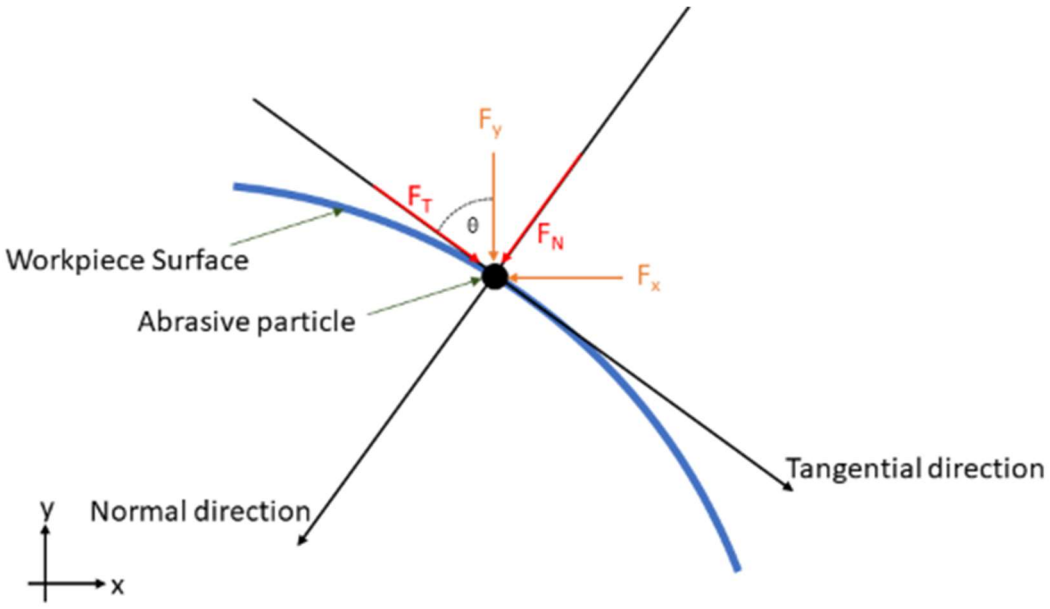

Figure 15: Free body diagram of the forces acting on an abrasive particle during the magnetic polishing process

2.2.2 Magnetic Fluid

Magnetic fluid or commonly known as ferrofluids are a particular class of smart materials that can be controlled in the presence of a magnetic field. These fluids are colloids of ferromagnetic nanoparticles (like magnetite Fe_3O_4) dispersed in a carrier fluid and stabilized with a surfactant. Therefore, this class of material exhibits fluid-like

behavior in the absence of a magnetic field source and solid like behavior in the presence of a magnetic field. On the microscopic scale, the van der Waals and magnetic forces are pervasive and must be balanced by coulombic forces by applying a surfactant that attaches to magnetic particles thus stabilizing the magnetic fluid [29], [30].Moreover, the carrier fluid has to be compatible with the surfactant to ensure the stability of the colloid.

2.2.3 Process Parameters

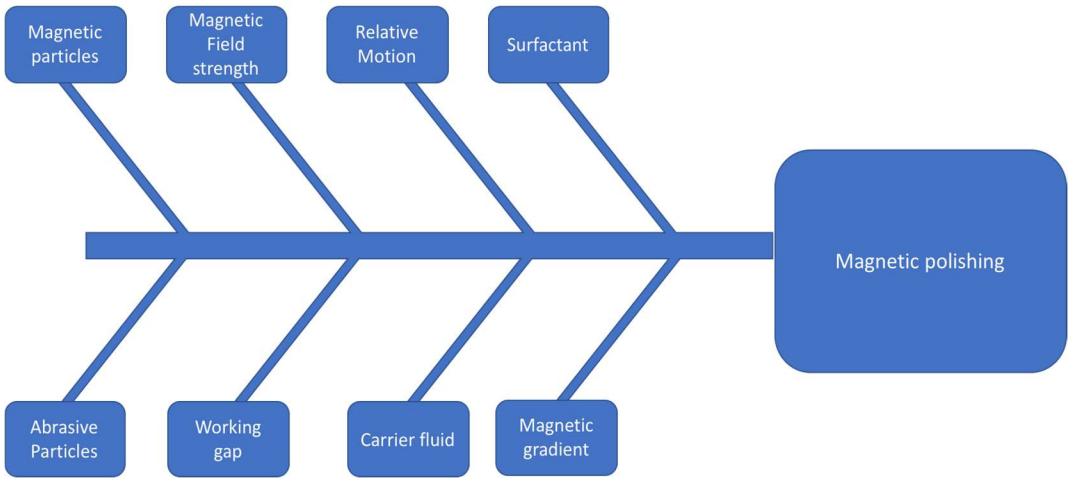

Figure 16: Elements influencing the quality of magnetic polishing process

Various elements influence (see Fig. 16) the surface finish generated by the magnetic polishing process. These include the magnetic particle types, abrasive particles type, and size, the distance between the magnet and the fluid and the relative motion between the workpiece and the fluid. In fact, great care must be taken when choosing the input parameters since they hold a significant influence on the process output. For example, the magnetic particles, surfactant, and carrier fluid must be compatible to create a stable colloid with good viscoelastic properties which will result in a better motion of the magnetic fluid thus resulting in a larger MRR.

2.2.4 Types of Magnetic Polishing

The use of a magnetic field for localized finishing was first recorded in 1938 for finishing the inner surface of welded joints of a barrel; specially to remove oxide scales using magnetic abrasive particles [31]. This setup is composed of a motor rotating the barrel and a fixed magnet underneath which concentrates the magnetic particles in one spot (see Fig. 17). The combined action of the rotation and the magnetic force on the abrasive particles creates a polishing action.

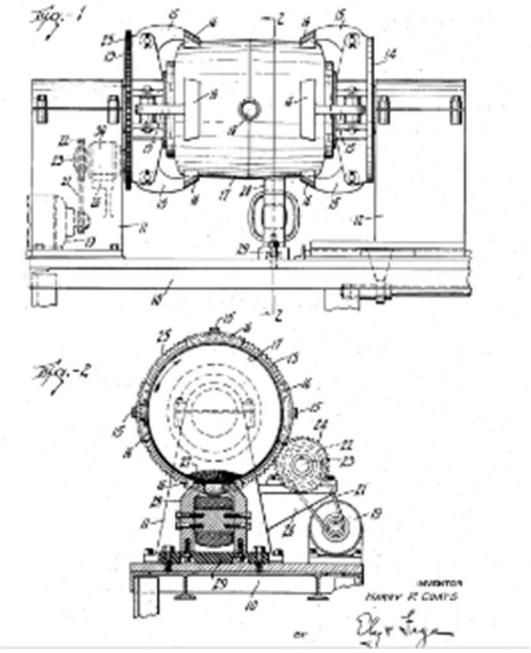

Figure 17: Schematic of system to polish internal surfaces of barrels with Ferrofluids (Reprinted from [31])

After almost half a century, it was Kordonski [7] who used magnetorheological fluids (MRFs) for finishing of optical glasses (see Fig. 18). In this process, a convex workpiece secured at a fixed position from a moving flat belt thus forming a converging gap. An electromagnet, placed under the belt at a fixed gap, generates a non-uniform magnetic

field thus providing the necessary magnetic gradient to stiffen the MRF. Combining the high shear stress of the MRF under the magnetic field with the lateral velocity provided

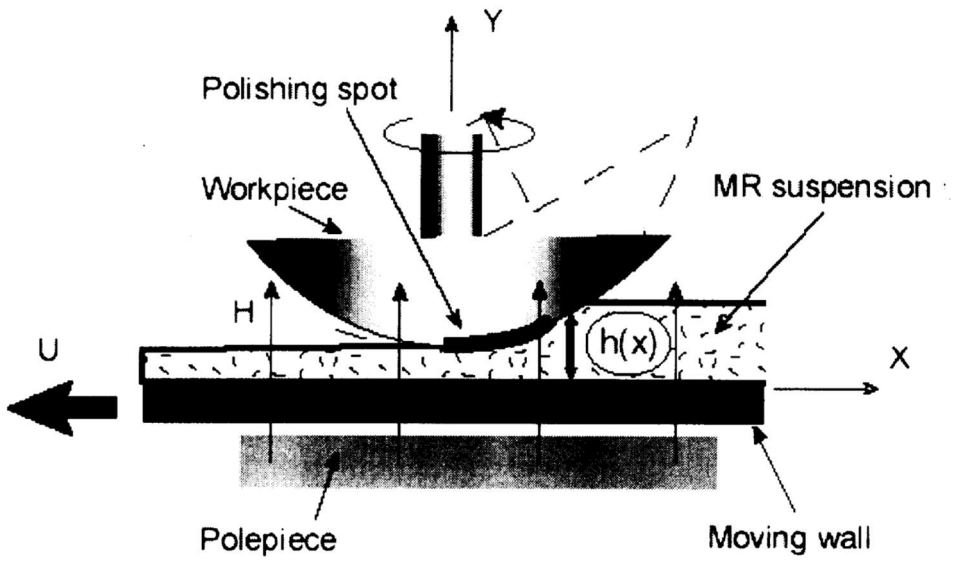

Figure 18: Schematic showing a magnetic polishing setup to finish curved lenses (Reprinted from [7])

by the conveyor belt, this process is capable of creating very high finish glass pieces. The belt also circulates the fluid which reduces the separation of the fluid, reduces heat effects and flushes the abraded glass particles thus increasing the quality of the surface. MR fluid utilized is composed of 55% water (carrier fluid), 36% carbonyl particles (magnetic particles) and 6% cerium oxide (abrasive particles) and 3% stabilizer (surfactant). Subsequent efforts focused more on the global finishing using magnetorheological fluids and much broader classes of magnetic fluids (MFs).

Alternative MF finishing methods have been developed based on employing different magnetic configurations as well as different variants and concentration of magnetic abrasives and fluids [32]–[35].

For example, Shinmura et al. [32] used bonded magnetic abrasives to polish steel and silicon nitride cylinders. The bounded particles were made from a mixture of 5μm pure iron and aluminum oxide particles at 4:1 weight ratio.

This mixture is then sintered at high temperature and pressure conditions (1600 K and 5Mpa) and then mechanically crushed and controlled to small size with a screen. This study also investigated the use of cast iron balls coated with diamond particles as a new type of magnetic abrasive particles (see Fig. 19) where the diamond particles are electrodeposited randomly on the surface of the balls. This was attempted with different size iron balls and different size diamond particles. Polishing with these particles improved the surface roughness of Si3N4 samples from 0.45um to 0.04 um. The study also showed that the surface roughness increases as particles of diameter “D” increased along with the grain diameter “d.”

Fox et al. [33] investigated the effects of using loose magnetic abrasives in cylindrical magnetic abrasive finishing process where the workpiece is placed between two magnets with opposing poles and in contact with the magnetic particles which form a flexible brush. The workpiece is then rotated (see Fig. 20) to induce polishing. It was noted

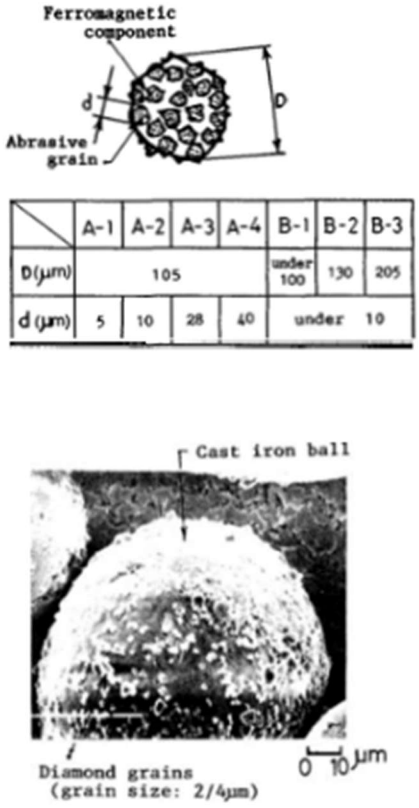

Figure 19: SEM micrograph of a cast iron ball bonded with abrasive particles using sintering (Reprinted from [32])

that this method increases the material removal rate (MRR) but results in a rougher surface. It was also determined that (a) imparting axial vibration to the workpiece resulted in a better surface finish, and (b) increasing the magnetic flux density yield a better MRR and surface finish [33].

Kim et al. [34] used a pressurized jet of magnetic abrasive particles through a nozzle to finish internal surfaces of a workpiece with a non-circular cross-section(Fig. 21).

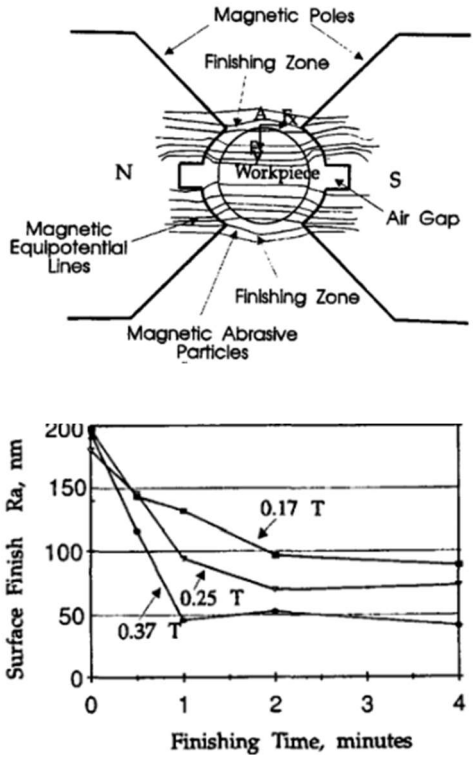

Figure 20: Schematic showing a barrel magnetic polishing with unbounded magnetic particles (Reprinted from [33])

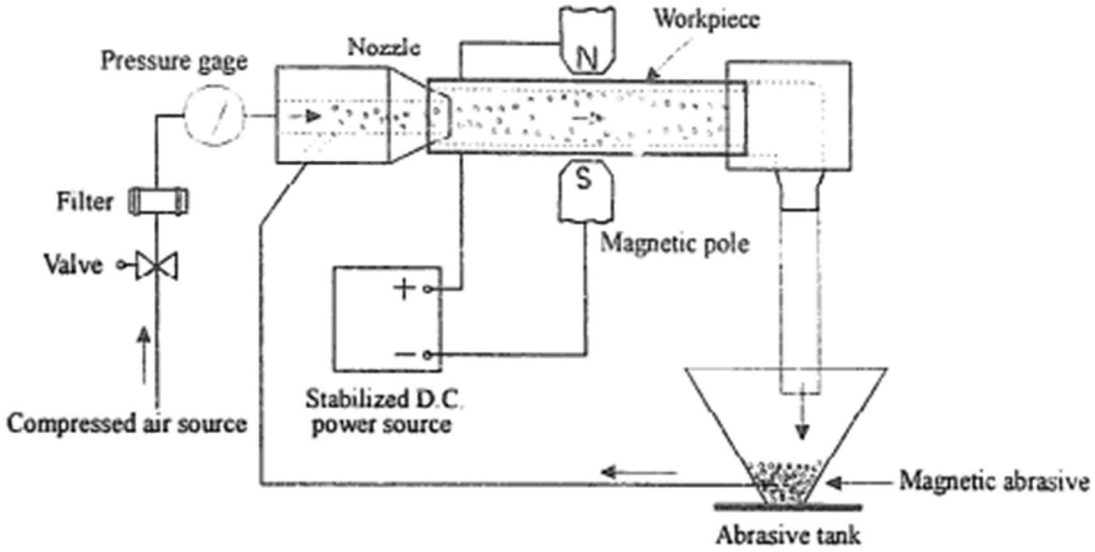

Figure 21: Schematic showing the magnetic jet polishing process (Reprinted from [34])

Yamaguchi et al. [35], employed MRF to finish the internal surface of a capillary tube. Although magnetic field strength was used to apply the necessary downforce, the workpiece (capillary tube) was mechanically rotated to generate the relative motion between the magnetic abrasives and the internal surface (Fig. 22). In addition to this, the finishing of complexly shaped tubes using this principle required specialized robotic arms to create the necessary relative motion between the abrasive particles and the workpiece surface.

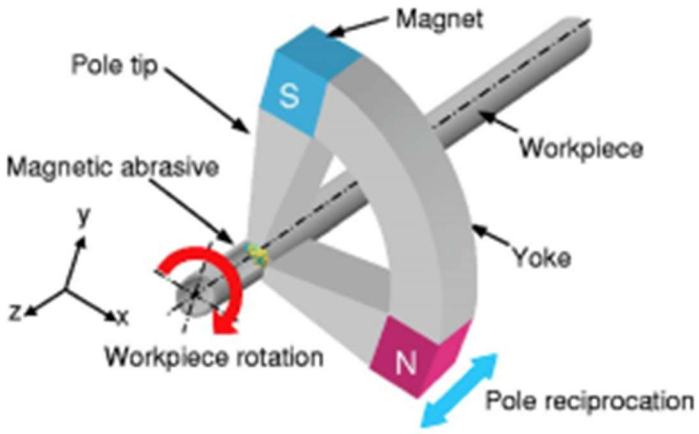

Figure 22: Schematic showing the magnetic polishing of capillary tubes process (Reprinted from [35])

More recently, Jain and Sidpara [36], demonstrated a methodology to polish free-form geometries to nanometer roughness using CNC milling machine connected to a neodymium magnet that serves at creating a flexible ball end MR finishing tool(Fig. 23). The diameter of magnetic finishing tool was kept sufficiently small so that the contact area was "locally flat." A specific tool path was then generated following the workpiece geometry, to polish the whole region while continuously varying the z-axis. However, the

downforce was provided using the finishing tool, rather than the magnetic strength. Other methods implemented to achieve localization or internal finishing involve controlling the geometry, shape, and placement of magnetic tool [1], [36], masking, magnetic abrasive jet finishing [34].

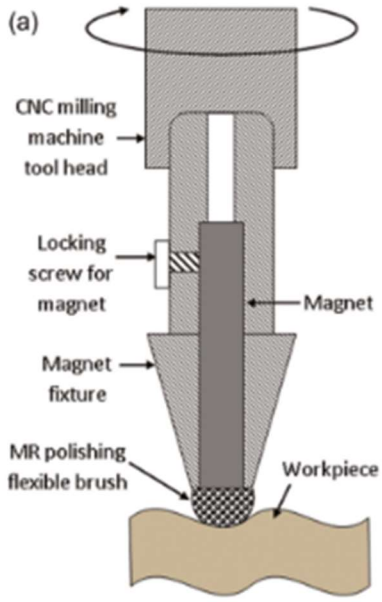

Figure 23: Schematic of CNC milling machine connected to a neodymium magnet that serves at creating a flexible ball end MR finishing tool (Reprinted from [36])

Sato, Wu et al. 2010 [37], , proposed a method to polish 3D features. However, instead, the workpiece is composed of flat surfaces at different heights which are far from freeform geometries. However, one of the significant contributions of their work was to demonstrate that dynamic magnetic fields are far more effective than static magnetic fields in polishing flat geometries at different heights. However, this method cannot be applied to free-form polish surfaces locally (Fig. 24).

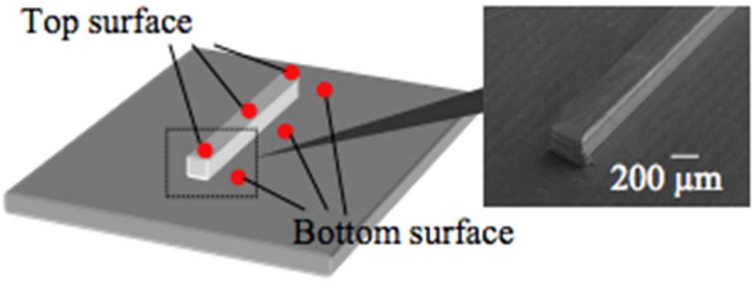

Figure 24: Magnetic polishing of 3D flat features (Reprinted from [37])

Guo, Wu et al. [38], showed the spot polishing of flat geometries in the presence of dynamic magnetic fields which was achieved by rotating the magnet fields and by its shape. They studied the variation of the forces acting the MRF (pressure and shear stress) with changing the working gap between the workpiece and magnet (Fig. 25). In particular, the spot size is limited to the size of the magnet and the spread of magnetic slurry. To vary the spot size, the magnet configuration and size had to be changed.

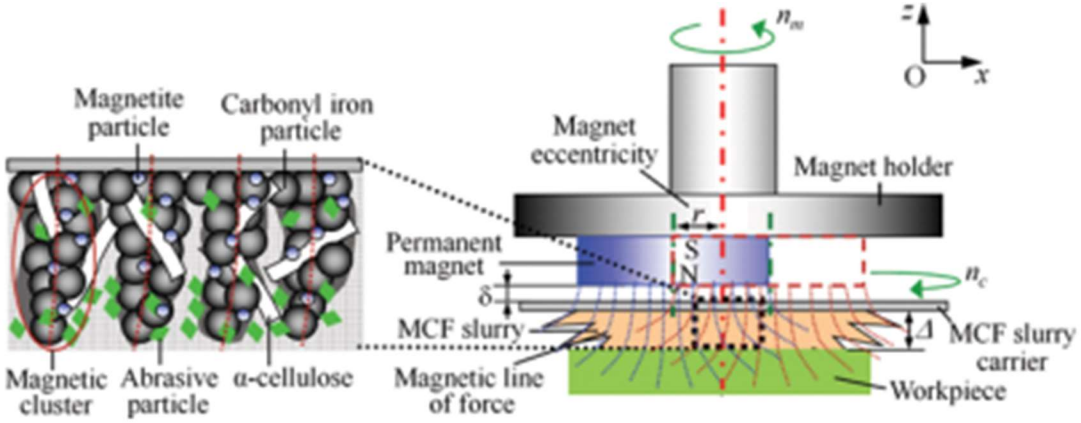

Figure 25: Schematic of magnetic polishing process with dynamic magnetic field (Reprinted from [38])

2.2.5 Gaps in Magnetic Polishing

Most of the current implementations of MF finishing methods either rely on some external mechanism to apply the necessary downforce and rotating parts to induce relative

motion between the workpiece surface and the abrasive mixed-MF. This significantly hinders their applicability to free-form and hard-to-reach geometrical surfaces. In addition, localization of the finishing action is also constrained by the geometrical aspects of the external mechanism/part used to induce the required downforce and relative motion. Although significant effort has been made towards developing specialized tools and configurations for example developing specialized robotic arms or CNC machines, less emphasis has been made on understanding and creating spatiotemporally varying magnetic fields without having movable parts to harness and optimize the visco-elastic properties of MFs, and therefore has not been employed to achieve localized finishing of free-form surfaces. Nonetheless, recent developments in transformation optics based magnetic concentration along with advances in tunable rheological properties, hydrodynamics of the MRFs, and electro-permanent magnets (EPM) [3], [4], [39], [40] offer exciting possibilities to simultaneously control the local dynamics (flow and downforce) as well as rheological properties by varying the magnetic strength and localization in space and time.

2.3 Magnetic Field Concentration

Spatiotemporal variation and concentration of magnetic field lines are critical to allow MFs (a) to stiffen in the presence of concentrated magnetic field lines adequately and consequently exert the required shear stress and normal force at desired locations to cause material removal, (b) flow to hard-to-access regions and execute sloshing action without the need for additional moving parts. In addition to this, abrasive-mixed MFs need to stay as a cohesive mixture (e.g., the abrasives should not segregate from the magnetic

matrix) and expose more abrasives towards the surface intended to be finished. In this section, we present a detailed overview of the concept of magnetic concentration along with the electro-permanent magnet configuration to achieve the aforementioned functionalities.

2.3.1 Physical Principle of Magnetic Field Localization

To localize and concentrate the magnetic field lines at an arbitrary location in space, we borrow the concept of magnetic energy harvesting and concertation proposed by Navau et al. [41]. It is in fact, an adaptation of the principle of Transformation Optics (TO) a novel approach that allows customizing the path of electromagnetic waves by reconfiguring the corresponding space by partitioning into regions of varying permittivity and permeability. A simple realization of this principle is the distorted path of magnetic field lines or electromagnetic ray, such as light, when incident on one face of a sandwich of glass slabs with varying refractive indices as shown in Fig. 26. TO takes advantage of the form-invariance of Maxwell's equations under any space-coordinate transformation, as discussed in the following subsection, to achieve a specified controlled pathway [42].

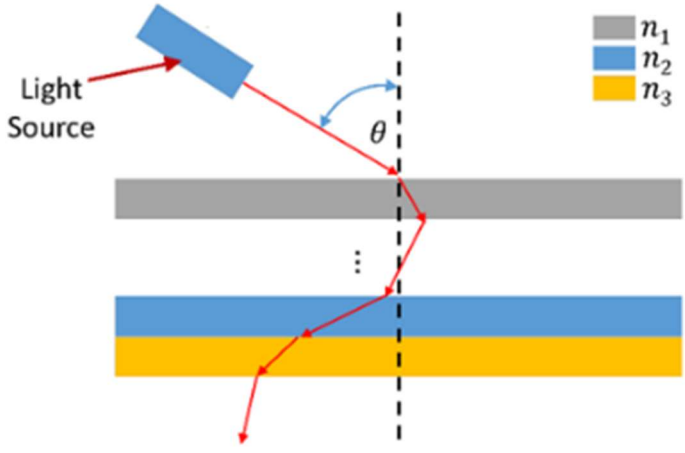

Figure 26: Schematic showing the distortion in the light ray path when transmitted through a sandwich of glass slabs with different refractive indices, n1,2 and n3. (Reprinted from [51])

These transformations can be achieved via specially engineered "metamaterials" (e.g., optical filters) that have different permeability values at different points to allow the manipulation of the electromagnetic waves in space, and therefore, create the desired spatial variation.

Recent simulation studies [43]–[45] with uniform magnetic fields demonstrated that magnetic field lines also respond to the change in permeability of space and could be governed by the principles of TO. By locally modifying the magnetic permeability of space, it is possible to harvest and concentrate the magnetic energy at the desired location in space. In the next subsection, we will discuss Maxwell's equations that govern the principles of transformation optics and magnetic concentration using an example.

2.3.2 Magnetic Concentration and Harvesting

Maxwell's equations as given in Eq. (1) are invariant to coordinate system transformation [42]

$$\nabla \times \mathbf{E} = -\mu_r \mu_0 \, \partial \mathbf{H} / \partial t \qquad \textbf{EQ 2-1}$$

$$\nabla \times \mathbf{H} = -\epsilon_r \epsilon_0 \, \partial \mathbf{E} / \partial t$$

where **E** is the electric field, **H** the magnetic field, μ_0 and ϵ_0 are the permeability and permittivity of vacuum, respectively and correspondingly, μ_r ,and ϵ_r are relative permeability and permittivity. Thus, when applying a transformation that distorts the space created by an orthogonal coordinate system, Maxwell's Equations retain their original form (Eq. (2)) where $\widehat{\mathrm{E}}$ and $\widehat{\mathrm{H}}$ are renormalized electric and magnetic fields and $\hat{\epsilon}_r$,and $\hat{\mu}_r$ represent the relative permittivity and permeability, respectively. However, the values of

permeability and permittivity are changed to account for the space transformations applied.

$$\nabla \times \hat{\mathbf{E}} = -\hat{\mu}_r \mu_0 \, \partial \hat{\mathbf{H}} / \partial t \qquad \textbf{EQ 2-2}$$

$$\nabla \times \hat{\mathbf{H}} = -\hat{\epsilon}_r \epsilon_0 \, \partial \hat{\mathbf{E}} / \partial t$$

This property of Maxwell equations is impressive since it allows for the preservation of the properties of the magnetic field of lines while redirecting them in a desired fashion by only changing the values of permeability (μ_r) and permittivity (ϵ_r) of the adjacent space. Transformation optics utilizes this principle to redirect light to achieve the intended functionality, e.g., to manufacture cloaking devices[43]–[46]. This has also been exploited to create a wide variety of magnetic devices such as magnetic lenses, magnetic concentrators, and magnetic shields [44], [46].

In this work, we explore specific transformations of space containing the magnetic field of lines that would allow harvesting magnetic field of lines from different regions in space and concentrate at an arbitrary location, specified apriori. Following the magnetic concentration principle and simulation models developed in the work presented by Navau et al. [41], we consider an infinitely long cylindrical shell with internal radii R_1, external radii R_2, thickness ξ, and relative angular and radial permeability μ_ρ and μ_θ, respectively. We show that by applying the concept of transformation optics, the magnetic field lines that would be in the region $\rho < R_2$ can be concentrated in the region, $\rho < R_1$.This structure divides space into three areas: interior space, the shell, and exterior space (see Fig. 27).

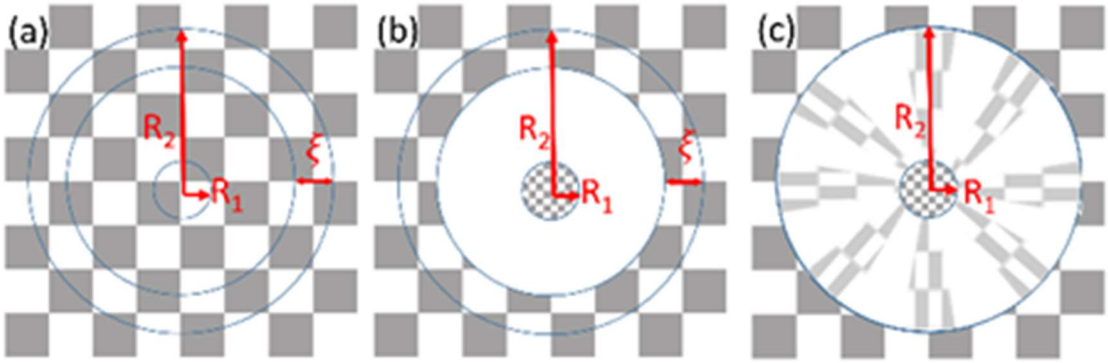

Figure 27: Space transformations corresponding to homogeneous anisotropic magnetic concentrating shell with an empty interior, (a) the original space (b) linear compression of the interior space, 0 < r < R2 − ξ (c) higher order polynomial expansion of the shell space, R2 − ξ < r < R2. (Reprinted from [51])

Let ξ be an infinitely small parameter such that the shell and the interior spaces are divided into two areas A_1 and A_2 as shown in Fig. 28(a) where,

$$\begin{cases} A_1: 0 < r < R_2 - \xi \\ A_2: R_2 - \xi < r < R_2 \end{cases} \qquad \textbf{EQ 2-5}$$

To achieve magnetic concentration, two sequential transformations are applied as described in [41]. First, the space A_1 is linearly compressed and is relocated in the interior space $(0 < r < R_1)$ (see Fig. 27(b)). Subsequently, a higher order transformation is applied to expend the space A_2 and relocate it in the shell space $(R_1 < r < R_2)$ (see Fig. 27(a)). After applying the TOs method on this transformed space, the necessary values of permeability to construct a magnetic concentration structure can be calculated. The interior space must have a permeability $\mu_{int.} = 1$ which means that this space must be empty to maximize the magnetic energy transfer to the interior space. The shell space needs an angular permeability $\mu_\theta \longrightarrow 0$ to avoid magnetic field leakage along the tangential direction and a radial permeability $\mu_p \longrightarrow \infty$ to redirect the field lines to the center. A material with such anisotropy does not exist naturally. However, advancements

in metamaterials offer a great solution since an alternating arrangement of ferromagnetic material, which provides a high radial permeability and diamagnetic material, with low permeability, is an excellent approximation to the results predicted by TO. Such a setup cancels the angular component of magnetic field consequently, preventing any magnetic leakage and transfers [41] the magnetic field energy out of the shell. Additionally, it concentrates the field lines in the interior space while also amplifying the magnetic field strength $H_{ext.}$ in the exterior space by a factor of R_2/R_1 .Thus, if the external magnetic field is uniform, the magnetic field in the interior $H_{int.}$ is given as

$$H_{int.} = \frac{R_2}{R_1} H_{ext.} \qquad \textbf{EQ 2-6}$$

However, if the external magnetic field is not uniform, $H_{ext.}$ depends on the position of the dipole and $H_{int.}$ becomes

$$H_{int.}(0, y) = \frac{R_2}{R_1} \frac{\eta}{2\pi} \left(y \frac{R_2}{R_1} - y_m \right)^{-2} \qquad \textbf{EQ 2-7}$$

where η is the magnetic moment per unit length of the magnet and the dipole is positioned at $(0, y_m)$.

3. COMPUTATIONAL MODELING AND SIMULATION[4]

Designing a prototype of a new localized magnetic polishing setup can be time and resource exhausting if relying solely on experimental studies. Thus, we took advantage of the finite element method which allows us to test many configurations and iterate multiple designs more efficiently. In This study, we have utilized the Finite Element Method Magnetics V 4.2 software which has 2D solver capable of analyzing planar and axisymmetric magnetic problems. In this section, we are going to introduce the fundamental equations necessary to describe a magnetostatics problem. Then, we are going to explain the mechanics of transforming our complex design problem into a solvable numerical problem via the finite element method, and finally, we are going to discuss the specifics of our models and their results.

3.1 Fundamental Equations

Our problem can be analyzed with a magnetostatics model since we are using static fields (or very low-frequency one) where the field flux (**B**) and the intensity (**H**) can be expressed as follows[47]:

$$\nabla \times \boldsymbol{H} = \boldsymbol{J} \qquad \textbf{EQ 3-1}$$

[4] Parts of the computational models and simulation are reprinted with permission from "Localized magnetic fluid finishing of freeform surfaces using electropermanent magnets and magnetic concentration" by Iskander El-Amri, Ashif Sikandar Iquebal, Arun Srinivasa, Satish Bukkapatnam, 2019. Journal of Manufacturing Processes,2018 https://doi.org/10.1016/j.jmapro.2018.05.026 , Copyright 2018 by Elsevier

$$\boldsymbol{\nabla \cdot B} = 0 \qquad \textbf{EQ 3-2}$$

where **H** and **B** are related by the following [47]:

$$\boldsymbol{B} = \mu \boldsymbol{H} \qquad \textbf{EQ 3-3}$$

However, if the material is a nonlinear the permeability can be expresses by the following equation [47]:

$$\boldsymbol{\mu = \frac{B}{H(B)}} \qquad \textbf{EQ 3-4}$$

The field flux **B** can be expressed in terms of potential vector **A** as follow [47]:

$$\boldsymbol{B} = \boldsymbol{\nabla \times A} \qquad \textbf{EQ 3-5}$$

by using equations (3-4) and (3-5) and substituting terms into equation (3-1) we can obtain the following relation

$$\boldsymbol{\nabla \times \left(\frac{1}{\mu(B)} \nabla \times A \right) = J} \qquad \textbf{EQ 3-6}$$

For a linear and isotropic material, the equation (6) reduces to

$$\boldsymbol{-\frac{1}{\mu} \nabla^2 A = J} \qquad \textbf{EQ 3-7}$$

In general, A is a vector with three components, however, in 2D planar or axisymmetric models, two of these components go to zero leaving only the component in the out of the page direction. Equations (3-6) is an elliptic partial differential equation which the FEMM solves for each element[47].

3.1.1 Finite Element Model Approach

3.1.2 Finite Elements

The finite element method can be applied to the problem domain, if we assume that there is no loss of magnetic energy i.e. [48]:

$$E_{input} = E_{stored} \qquad \textbf{EQ 3-8}$$

The energy is inputted to the system as a current density **J** and is outputted in a magnetic field **B** thus we can express the input and stored energies in the following equation [48]:

$$\frac{1}{2}\int \boldsymbol{J} \cdot \boldsymbol{A} dv = \int \frac{B^2}{2\mu} dv \qquad \textbf{EQ 3-9}$$

Let's call define F as the difference between E_{input} and E_{output} , thus F can be written as (for a linear magnetic field) [48]:

$$F = \int \left[\frac{B^2}{2\mu} - \frac{1}{2}\int \boldsymbol{J} \cdot \boldsymbol{A}\right] dv \qquad \textbf{EQ 3-10}$$

To apply the finite element method, the energy must be minimized. Thus, it is necessary to take the partial derivative of F with respect to A and set it to zero [48]:

$$\frac{\partial F}{\partial A} = 0 \qquad \textbf{EQ 3-11}$$

We can rewrite equation (3-10) in the following form [48],

$$\frac{\partial}{\partial A}\int \frac{B^2}{2\mu} dv = \int J dv \qquad \textbf{EQ 3-12}$$

To solve the previous equation, the finite element method divides the problem domain into small elements made from simple geometric shapes like triangles (see Fig. 28). These small triangles discretize the magnetic flux B plane, which lies in the (XY)

plane, into small areas. Meanwhile, the current density vector J and the potential vector A lie in the out of page direction. To solve for A, we utilize the first order triangular element shown in the figure below with vertices O, P, and Q representing the nodes at which the unknown A must be found. **A** can be expressed as a first order polynomial shape function over the (XY) plane:

$$A(x,y) = \sum_{i=O,P,Q} [A_i(a_i + b_i x_i + c_i y_i)] \qquad \textbf{EQ 3-13}$$

By expending the previous equation, we can obtain the constant coefficient matrix relation

$$\begin{pmatrix} a_O & a_P & a_Q \\ b_O & b_P & b_Q \\ c_O & c_P & c_Q \end{pmatrix} = \begin{pmatrix} 1 & x_O & y_O \\ 1 & x_P & y_P \\ 1 & x_Q & y_Q \end{pmatrix}^{-1} \qquad \textbf{EQ 3-14}$$

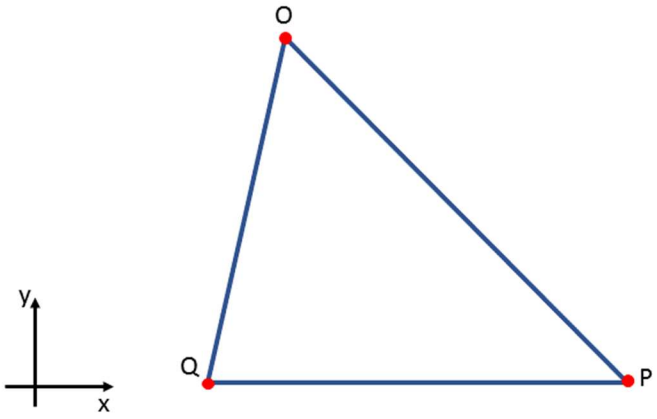

Figure 28:Triangular element used in the finite element to discretize the problem domain

Substituting the shape function into equation(3-12) , we obtain,

$$\int \frac{\partial}{\partial A_i}\left(\frac{B^2}{2\mu} - \frac{1}{2}JA\right) dv = 0 \qquad \textbf{EQ 3-15}$$

Taking the curl of **A,** we obtain

$$B^2 = \left(\frac{\partial A}{\partial x}\right)^2 + \left(\frac{\partial A}{\partial y}\right)^2 \qquad \textbf{EQ 3-16}$$

The final step of the finite element method is to find the stiffness matrix which can be expressed as:

$$\left(\frac{A_r}{\mu}\right)\begin{pmatrix} b_O b_O + c_O c_O & b_O b_P + c_O c_P & b_O b_Q + c_O c_Q \\ b_P b_O + c_P c_O & b_P b_P + c_P c_P & b_P b_Q + c_P c_Q \\ b_Q b_O + c_Q c_O & b_Q b_P + c_Q c_P & b_Q b_Q + c_Q c_Q \end{pmatrix}\begin{bmatrix} A_O \\ A_P \\ A_Q \end{bmatrix} = \left(\frac{A_r}{3}\right)\begin{bmatrix} J \\ J \\ J \end{bmatrix} \qquad \textbf{EQ 3-17}$$

where A_r is the area of the triangular element. The previous equation can be rewritten as

$$[K]\{A\} = \{J\} \qquad \textbf{EQ 3-18}$$

with K is the stiffness matrix, the vector J is given, and the A is the vector to be found.

3.1.3 Boundary Conditions

To find a unique solution for the model, it is necessary to the define boundary conditions. For the 2D planar magnetostatics models, a Dirichlet Boundary condition is applied where the value of the potential vector A is defined explicitly to be zero at the

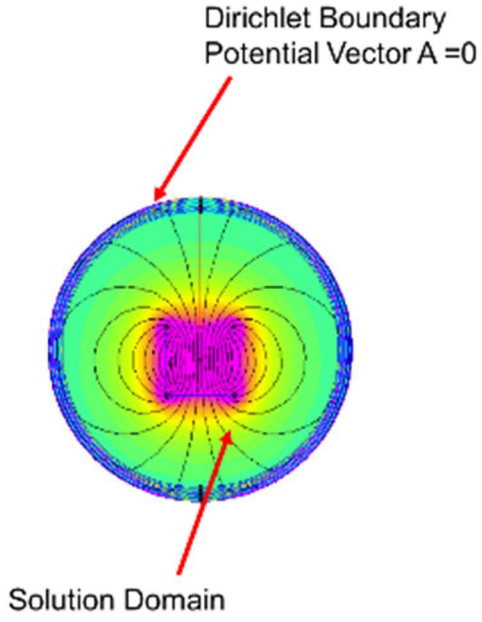

Figure 29: schematic showing the boundary and solution domain

boundary of the domain which is a region sufficiently far away from the source of the magnetic field where the magnetic field value would drop to zero [47], [48].

In the case of the axisymmetric models, the line passing through the center of the region has a vector potential **A** set to zero.

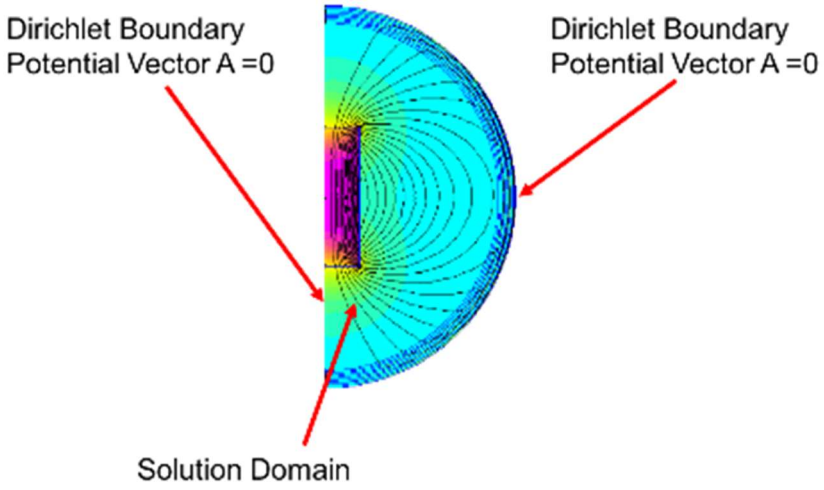

Figure 30: Schematic showing the boundary condition and the solution domain of axisymmetric model

3.1.4 Mesh

The FEMM solver utilizes a heuristic algorithm to define the optimal element number and size to ensure fast convergence of the model. The solver also adapts the mesh

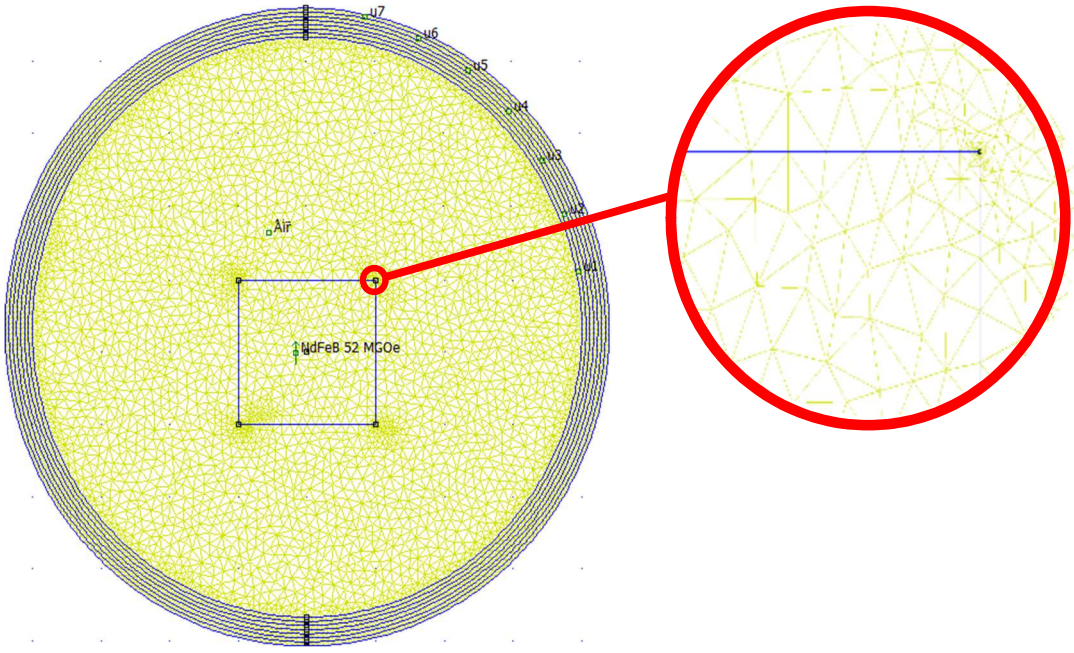

Figure 31: schematic showing the mesh created by the FEA software and the automatic element size adaptation

size depending on the geometry .i.e. smaller elements close to a corner or to curved edge while utilizing lager size elements in other position with less stress (see Fig. 31).

3.2 Models and Simulation Results

3.2.1 Magnetic Concentration Structure Model

Following the conceptual development in section 2.3 (discussing transformation optics), we implemented a model using air as the region of low permeability, whereas the high permeability region is created by using 1006 steel core with a broader base and a tapered tip. Two cylindrical grade N52 neodymium magnets, with a diameter of 0.75” and

a height of 0.75" are attached end-to-end to each of the steel core to amplify the magnetic field via the transformation optics principle described in Section 2.3. We chose to use cores in this fashion since they provide a broad base that can concentrate most of the field lines emanating from the pole of neodymium magnets and sharp tip to focus the lines at a localized spot. The output of the model is a density map of the magnetic field strength |**B**| (as shown in Fig. 32(b)). The model consists of 30400 nodes and 15381 triangular elements.

The density map shows a magnetic field concentration region surrounding the structure. The maximum magnetic field strength of 0.3T was recorded near the tip of the steel core, and the variation of the field strength as a function of distance from the pole is plotted in Fig. 32(b) (red profile). In contrast, it could be explicitly noted in Fig. 32(b) (blue profile) that the field strength is significantly weaker in the same region when the steel cores are removed. This shows that all or most of the magnetic field of lines emanating from the magnets are concentrated in the vicinity of the structure which ensures a high magnetic flux density thus a higher magnetic field strength.

The magnetic concentration setup, as we showed, is capable of creating intense magnetic fields that can be used to generate downforce in MFs which is necessary for material removal [1]. However, along with the sufficient downforce, it is necessary to have a relative motion between the workpiece and the magnetic fluid to create a polishing action. To achieve this functionality, we create a spatiotemporally varying magnetic field that would force the magnetic fluids to flow according to the magnetic gradient and therefore create a sloshing action. However, along with the sufficient downforce, it is

necessary to have a relative motion between the workpiece and the magnetic fluid to create a polishing action. To achieve this functionality, we create a spatiotemporally varying magnetic field that would force the magnetic fluids to flow according to the magnetic gradient and therefore create a sloshing action.

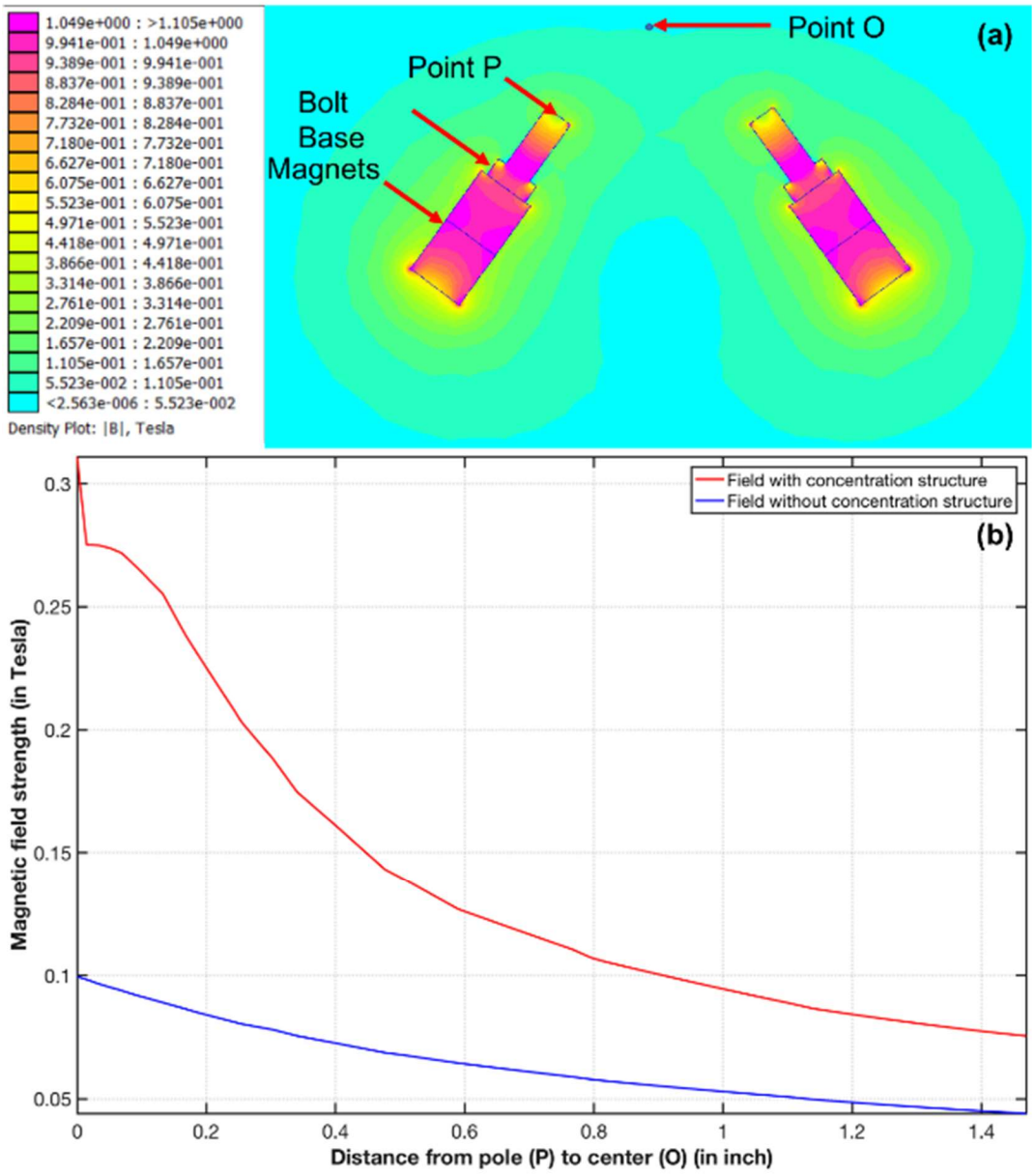

Figure 32: (a) Density map showing the field strength generated by the magnetic concentration Structure (b) Field strength measured in the vicinity of the structure and field strength measured without the structure

3.2.2 Modulating Magnetic Field Using EPMs

EPMs are a class of specialized permanent magnets that combine the high field

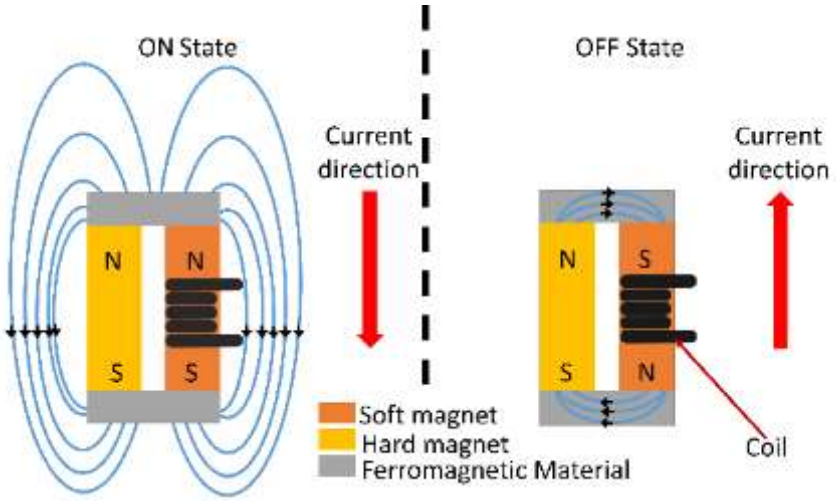

Figure 33: Schematic showing the ON state of EPM and the effect of current direction on the magnetic field lines (b) and OFF state of EPM and the effect of current direction on the magnetic field lines. (Reprinted from [51])

strength of rare earth permanent magnets with the polarity control of solenoids. These devices can display a high magnetic field in the ON state (no current passing through the solenoid) but will have weak or zero magnetic field if a current pulse is applied in the opposite direction. This allows the EPM to create a stronger magnetic field strength as well as to preserves the flexibility of conventional electromagnets to toggle the magnetic field on and off while being more compact and less energy demanding. Usually, EPMs are based on a combination of hard magnets (high coercivity) and soft magnets (low coercivity) connected by a ferromagnetic material on both ends. The soft magnet is wrapped with coils since it has a small hysteresis loop which requires less energy in reversing the direction of magnetization as compared to the hard magnet.

In the ON state (see Fig. 33(a)) , the soft and hard magnets have the same polarities, forcing the field lines out of the device thus creating a high magnetic force. In the OFF state (see Fig. 33(b)), current is applied through the coils around the soft magnet to reverse its polarity. Thus, both the hard and soft magnets will have opposite polarities, forcing the magnetic field lines to circulate through the ferromagnetic material. Consequently, there will be no noticeable magnetic force created by the EPM [3]. However, this design only allows to toggle the magnetic force between the ON and OFF states and does not increase the original magnetic field strength generated by the permanent magnets. Also, this design does not channel the field lines in the desired direction.

3.2.3 New EPM Design

To address the issues discussed in the previous section, we developed a new EPM design consisting of a combination of a steel core solenoid affixed to a permanent magnet. The steel core has a large base and sharp tip to channel most of the field lines generated by the permanent magnet along its axis, while also boosting the magnetic field generated by the coils. When the current generated field lines are in the same direction as the one generated by the permanent magnet, the resulting field holds a higher magnitude as a result of the constructive superposition of both fields. When the current is reversed, the device outputs a very low to zero magnetic field due to both fields canceling each other. This property of our design creates sharp gradients which create a high spatiotemporal variation of the magnetic field. The novel EPM design increases the range of action of the magnetic field away from the magnetic field source which increases the overall magnitude of the magnetic gradient. We created an axisymmetric model to study the EPM magnetic field

strength. As shown in figure 34 (a), the magnetic fields generated by the coils is opposing the field generated by the permanent magnets. In figure 34 (b) , the magnetic fields created by the coils is in the same direction of the field generated by the permanent magnets. We can observe that the magnetic field region is increased with the use of the EPM which allows to extend the magnetic force magnitude away the source.

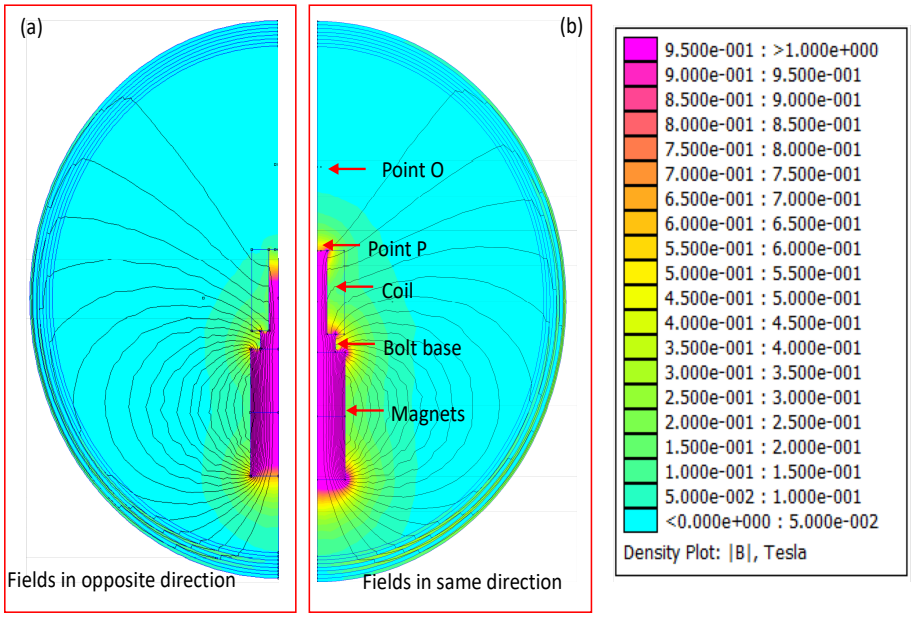

Figure 34: Simulation output showing low magnetic field when the current induced magnetic field is in the opposite direction of the magnetic field as generated by the hard magnet (b) when the current induced magnetic field is the same direction as the magnetic field generated by the hard magnet.

To determine the appropriate size of the steel core, we have created a simulation model that changes the dimensions L1, L2, D1 and D2 shown in the figure below (see Fig. 35).

We give our model a starting size for the core with which we can verify the magnetic strength experimentally and then the program fixes three parameters and changes one at a

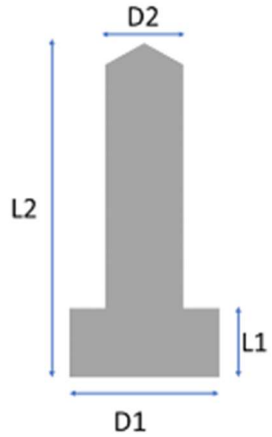

Figure 35: Schematic of the EPM Core model

time. The data for each parameter change is recorded and a plot of the magnetic field strength vs the fixed parameter is generated. These four plots help in determining the parameters values with the highest increase of the magnetic field strength generated at the tip of the EPM (Fig. 36, Fig .37

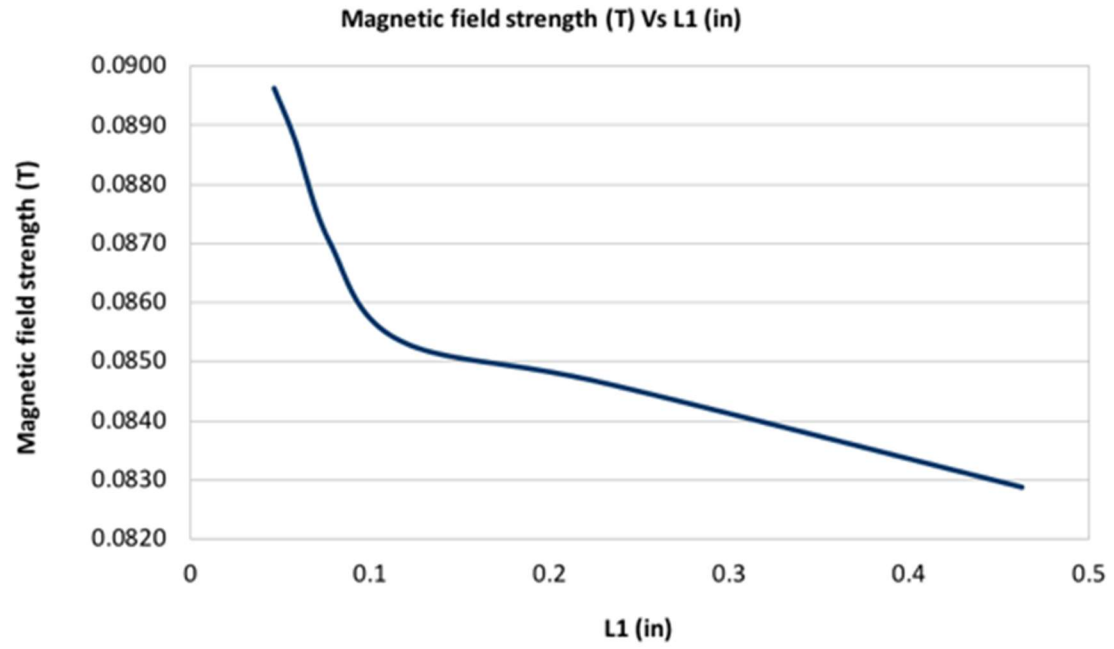

Figure 36: Magnetic field strength at the tip of the core vs L1 size

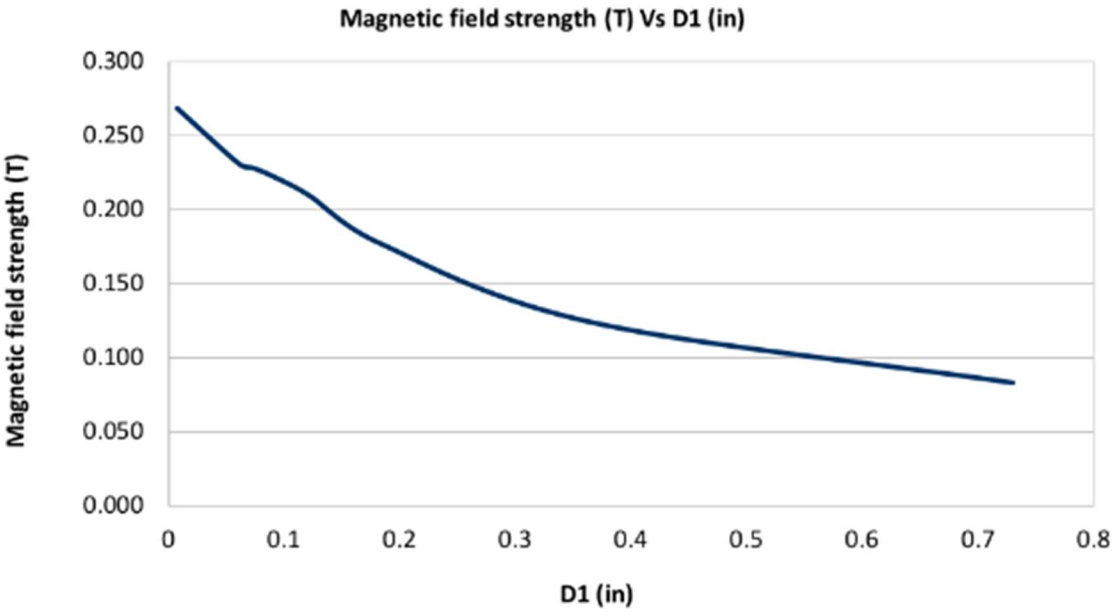

Figure 37 Magnetic field strength at the tip of the core vs D1 size:

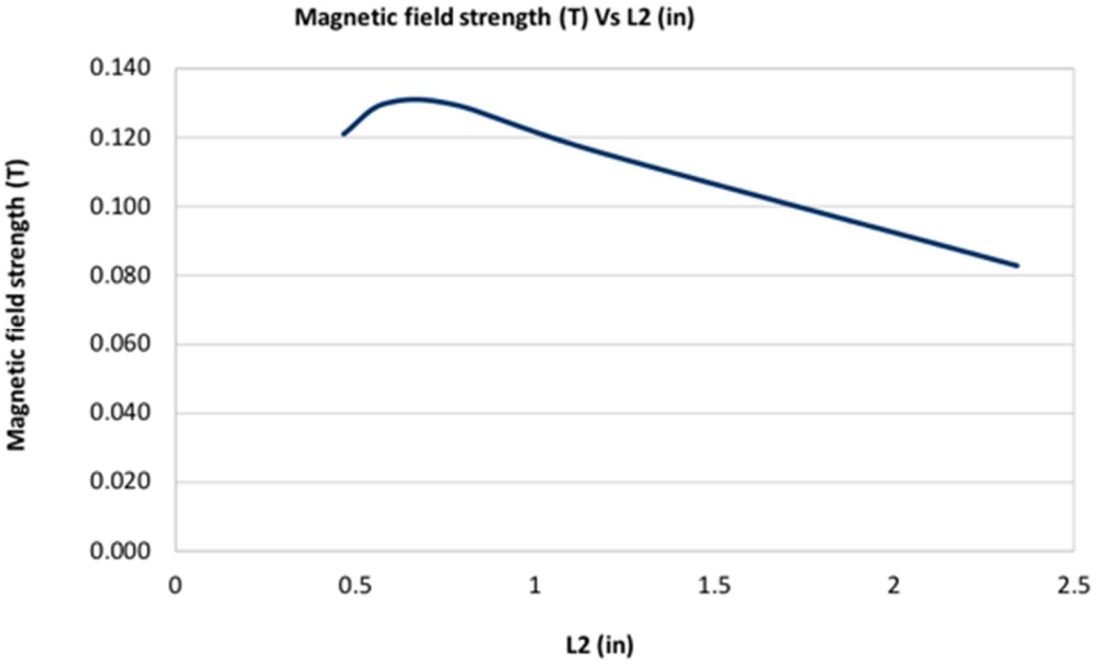

Figure 38: Magnetic field strength at the tip of the core vs L2 size

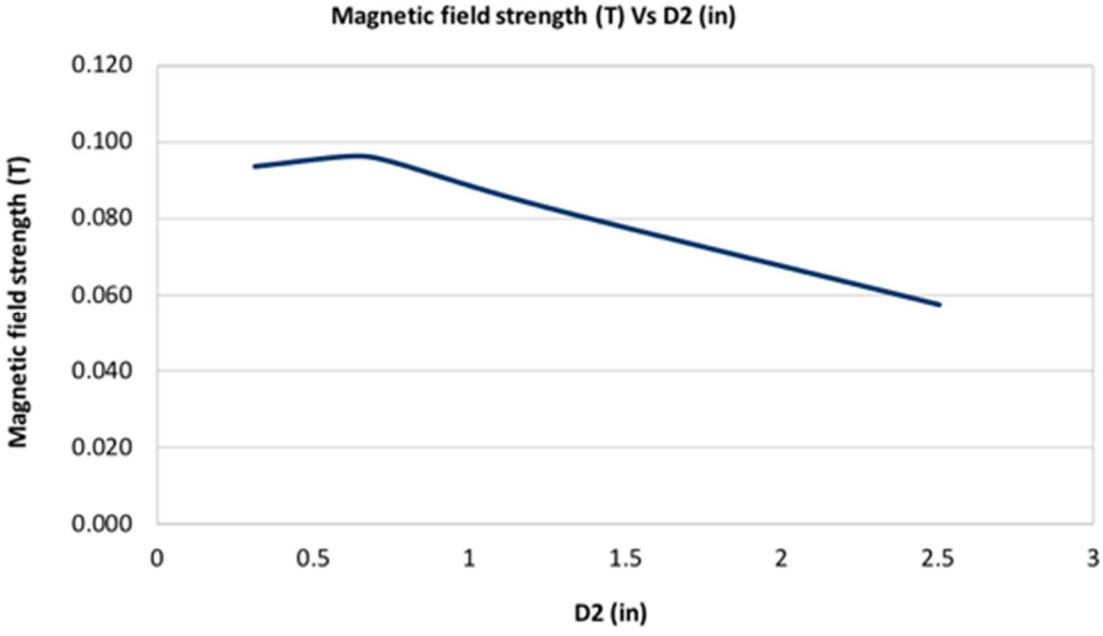

Figure 39: Magnetic field strength at the tip of the core vs D2 size

The initial parameters used where L1=0.211”, L2 =1.2015”, D1 =0.288”, D2=0.65” (see Fig. 36, 37, 38 and 39) with a magnetic field strength of B= 0.25T. From there, the model changes the values of the geometric parameters and plots the results. We choose the parameters values that allows us to have an increase of the magnetic field at the tip of the steel core while also making sure that the field strength is not too high to be countered by the field generated by the solenoid.

To determine the necessary number of coils necessary for a functioning EPM, we have created an axisymmetric model consisting of a steel core and the neodymium magnets (as discussed previously) while adding copper wire wound around the core. The model changes the number of copper wire turns in each iteration while also changing the current direction and plots the magnetic field strength at the tip. Using this approach, we can determine the number coils necessary to create the toggling action of the EPM without extensive experimental studies. As shown in Fig. 40, we can see that increasing the number of turns while the magnetic fields of the electromagnet and the permanent magnet are in the same direction generates a higher combined field (red profile). However, when reversing the direction of the current, we see that the magnetic field strength decreases until reaching 600 turns. Nevertheless, increasing the number of turns results in a constructive interaction between the fields thus increasing the overall magnetic field strength (blue profile). Thus, using a value of 600 turns yields a good balance between increasing the value of the generated field to .5T thanks to the constructive interference of the fields; however, the total EPM field drops to almost zero due to the deconstructive interference of the fields.

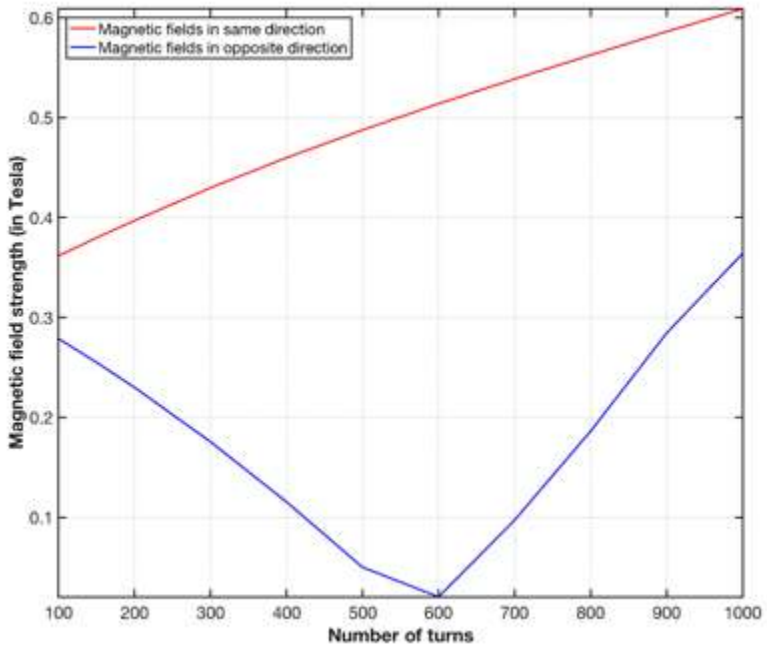

Figure 40:Magnetic field vs the number of copper wire turns around the core of the EPM

3.2.4 Spatiotemporal Variation of Magnetic Fields

Spatiotemporal variation of magnetic field strength allows the MFs to generate a sloshing action [1], [49] that is necessary to perform the material removal. Most of the conventional MF polishing approaches either use an external means to mechanically to generate the relative motion between the magnetic abrasive brush and the workpiece or utilizes additional rotating components to create the spatiotemporal variation of magnetic fields. This significantly hinders the applicability of these approaches in the finishing of hard-to-access, free-form surfaces. To address these challenges, we use the EPM configuration discussed in the previous section since it can toggle the magnetic field direction, thereby changing the magnetic strength from one pole to another. In effect, this

creates a sloshing effect in the fluid. To validate the toggle action, we developed two simulation models as shown in figures. 41(a) &41 (b)

From the computational model, we can measure the field strength profile between

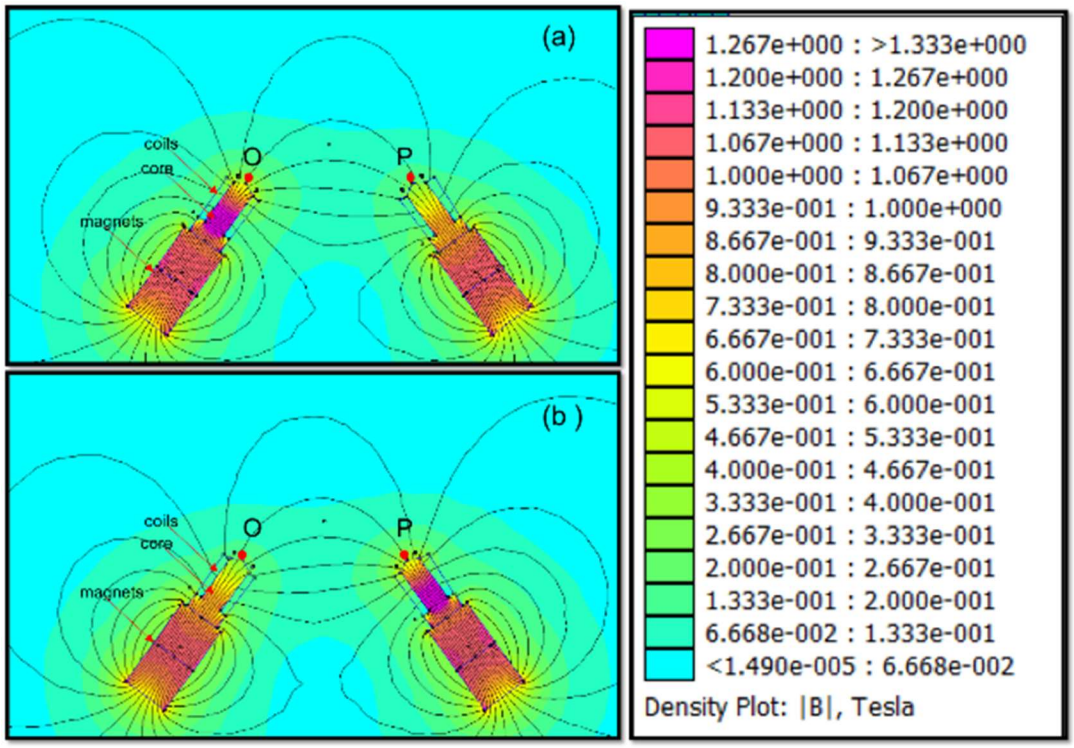

Figure 41: (a) Magnetic field density map when the left EPM is ON and right EPM is OFF (b) Magnetic field density map when the left EPM is OFF and right EPM is ON

points O and P (Fig. 41 (a) & (b)) while alternating the ON/OFF state between the two EPMs. The switching action shifts the direction of the magnetic field gradient depending on the respective state of EPMs. Also, the switching frequency controls also the gradient amplitude. Using a low frequency and 3A current, the magnetic field near the pole was amplified to 0.5T on the high side and 0.1T on the low side (see Fig. 42). Toggling the EPM states (as shown in Fig. 42) results in a sharp gradient that moves from point O to point P.

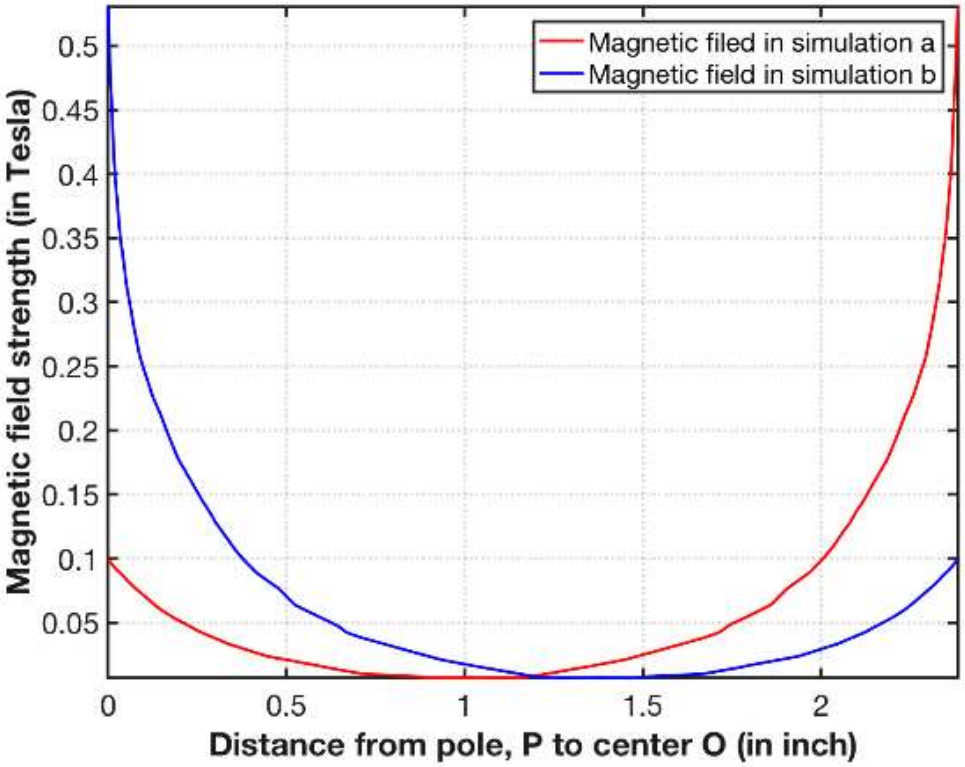

Figure 42:Magnetic field strength from point O to P when current direction is flipped

4. EXPERIMENTAL SETUP AND DETAILS[5]

The magnetic polishing experimental setup can be divided into four main subsystems, namely:

The electro permanent magnet assembly, the electronic controller, the magnetic fluid and the cooling system (See Fig. 43). In this section, we will describe the main function of each subsystem explain the function of each component.

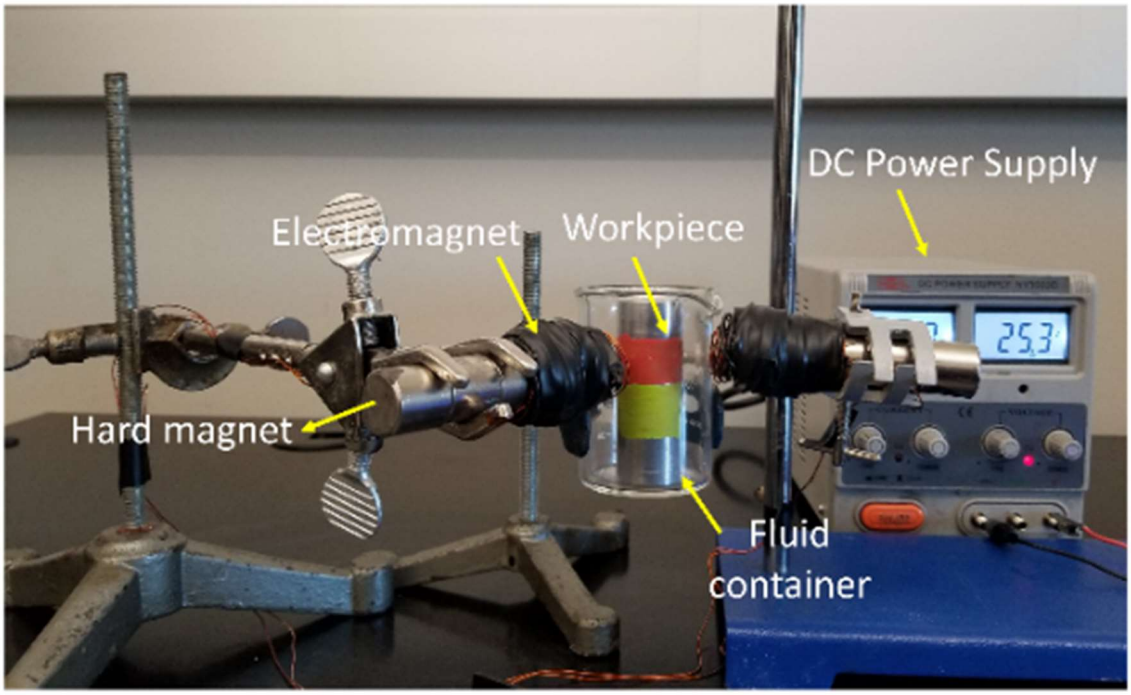

Figure 43: Photograph showing the experimetal setup(Reprinted from [51])

[5] Parts of the experimental setup and detail are reprinted with permission from "Localized magnetic fluid finishing of freeform surfaces using electropermanent magnets and magnetic concentration" by Iskander El-Amri, Ashif Sikandar Iquebal, Arun Srinivasa, Satish Bukkapatnam, 2019. Journal of Manufacturing Processes,2018 https://doi.org/10.1016/j.jmapro.2018.05.026 , Copyright 2018 by Elsevier

4.1 Electro Permanent Magnets

Based on the results from the FEM models presented in the previous section, we built the EPM device comprised of two N52 grade neodymium magnets with Ø0.75" and height 0.75" affixed axially to an electromagnet. The electromagnet is composed of 500 turns of 22 AWG copper wire coiled around a 1.2" long 1006 steel bolt (carbon content <0.08%) (see Fig. 44). The 1006 steel is a excellent choice for the EPM's core since it has a low residual magnetic field which allows an easy magnetization/demagnetization cycles

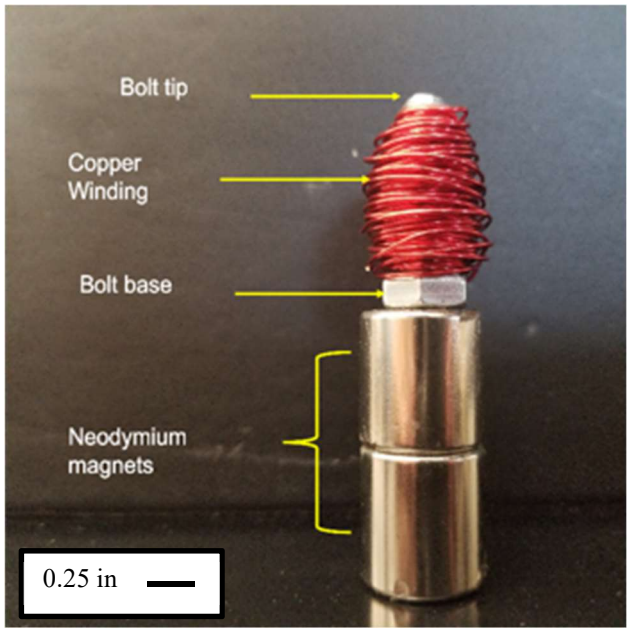

Figure 44:Photograph showing the different components of the new EPM design.

thanks to its low carbon content. We chose the 22 AWG wire since they can dissipate the heat generated by the high current while also having a small enough diameter to ensure a more compact EPM. Neodymium magnets are the strongest permanent magnets compared to their size, thus using them is a good choice to create a compact yet strong EPM.

4.2 Cooling System

The main issue faced when using electromagnets with high currents is heat. So, to control and stabilize the heat emitted by the EPMs, the use of a cooling system is deemed necessary to protect the setup from sparks and heat related issues.

The cooling system is composed of a thermoelectric cooling device that uses the Peltier effect to transform current into a heat gradient where one side of the device gets cooled down while the other side heats up. The Peltier device is attached to aluminum heat exchanger on the cool side and to a fan and fins on the other side. The heat exchanger is attached through vinyl tubing to the EPM housing and to a DC pump that circulates mineral oil to extract heat from the magnets. The hot fluid then, goes through the heat exchanger where it is cooled by the Peltier module. The Peltier module then transfer the heat through the on the hot side (see Fig. 45 and 46).

We chose mineral oil as the coolant because it is nonconductive thus eliminating the risk of short circuiting the setup and oxidizing the EPMs coils and cores.

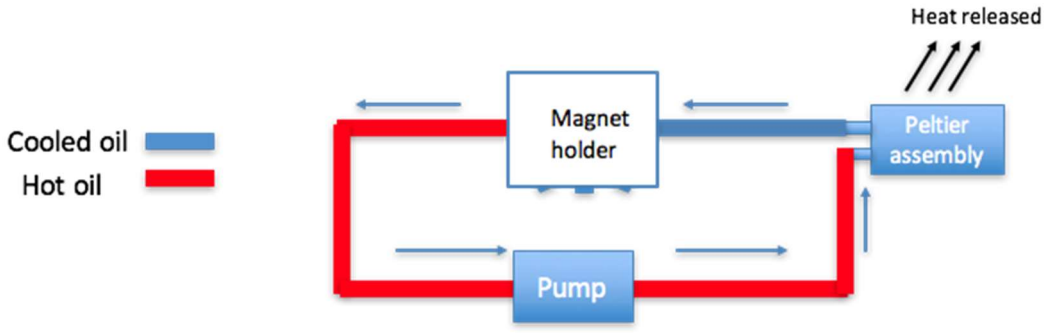

Figure 45: Schematic of the Cooling system heat flow

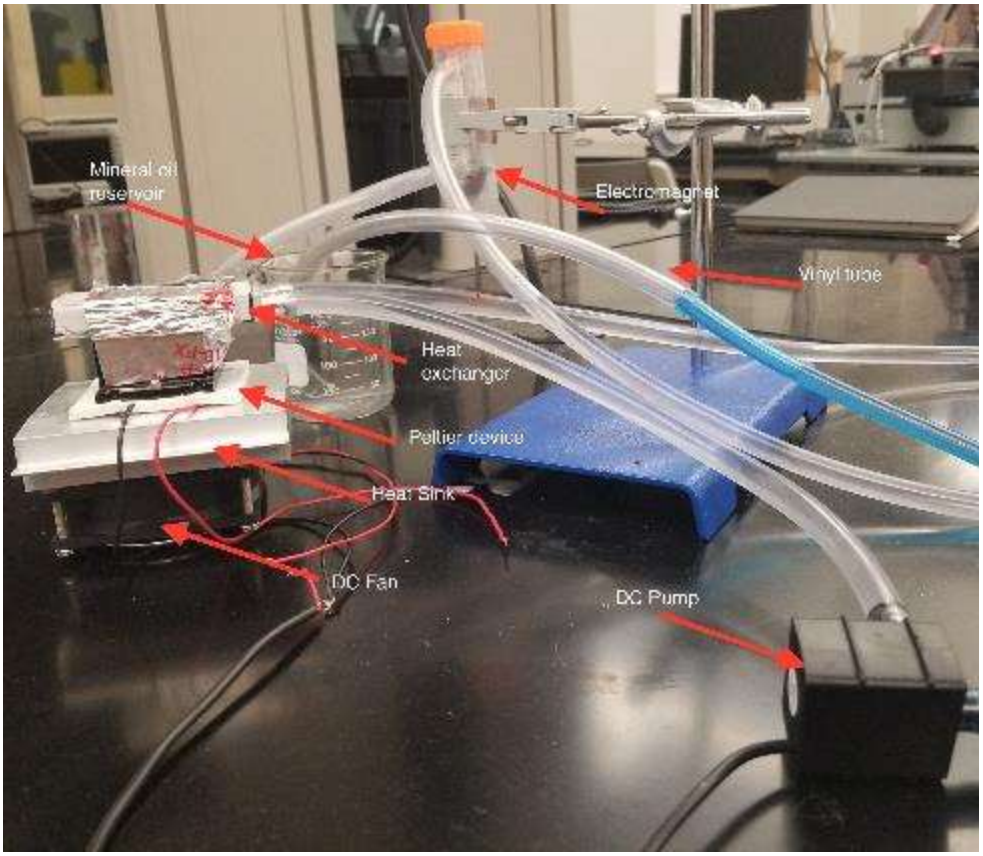

Figure 46: Photograph of the cooling system

4.3 Electronics Controls

The H bridge circuit (see Fig. 47) is comprised of a dual H bridge, capable of controlling two EPM, mounted on Arduino Uno microcontroller. The microcontroller outputs a +/-5V pulse width modulation signal which serves as an input to the H bridge circuit (see Fig.48).

When the input signal has a value of 5V, the transistors Q1 and Q4 allow the current to flow through which results in a clockwise current. However, when the input signal has a value of -5V, the transistors Q2 and Q3 allow the current to flow through in

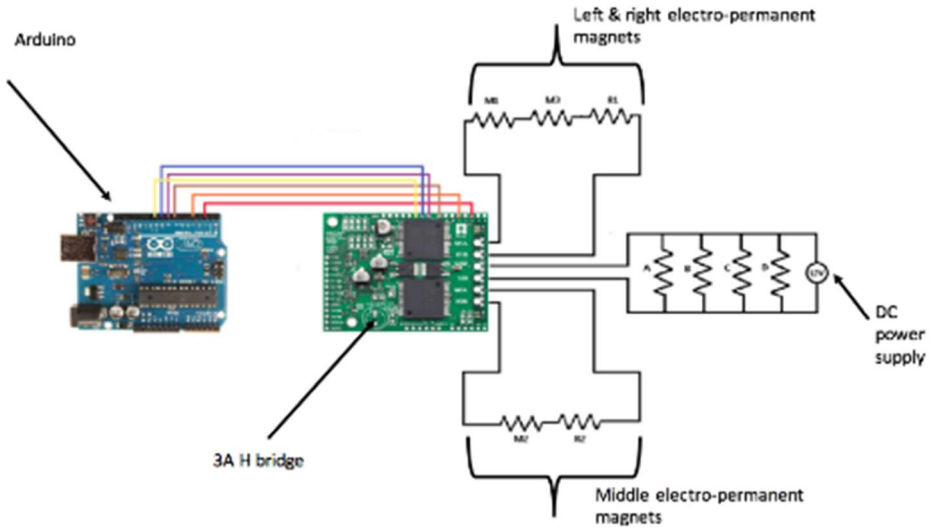

Figure 47*: Schematic showing the circuit controlling magnetic polishing process*

the counterclockwise direction (see Fig. 49). The H bridge toggles between clockwise and counter clockwise 3A current which controls the direction of the induced magnetic field.

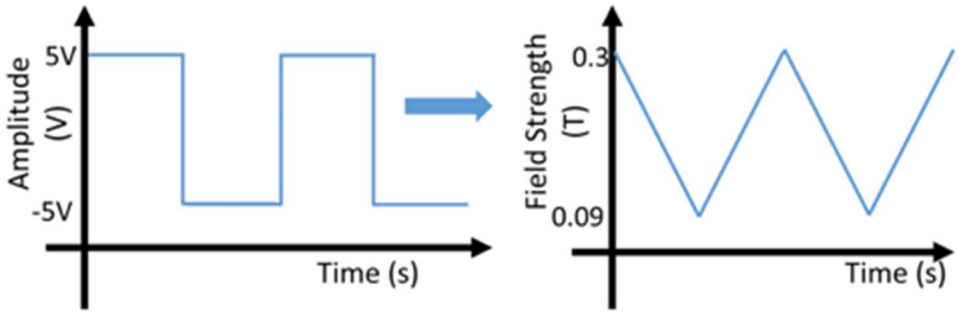

Figure 48: Magnetic field gradient generated by the EPM subject to a pulse with modulation signal (Reprinted from [51])

The H bridge circuit can support a pulse width modulation signal up to 20 kHz which offers a wide range of frequencies to test the sloshing motion of the MF. The circuit is powered by a DC power supply and is fitted with resistors to protect the electronics (see Fig. 47).

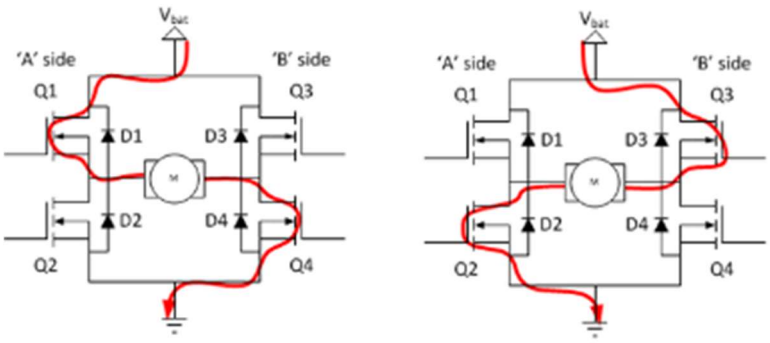

Figure 49: Schematic showing the circuit of an H bridge

4.4 Ferrofluid

The ferrofluid used in our experiments was made with 50 nm magnetite particle. The particles are then mixed with an ammonia solution and the mixture is heated until ebullition (100°C).

The surfactant needs to be adequately chosen to bond with the superparamagnetic particles to overcome the gravitational force (causing sedimentation) and the inter particles magnetic interactions (causing agglomeration). In this case, we chose oleic acid since it is safer than other commonly used surfactant.

The solution is kept at a constant temperature (100°c) to give the oleic acid molecules the necessary energy to bond with the magnetite particles. After 90 min, the solution is cooled down and carrier fluid is added. The carrier fluid characterizes the viscosity and consequently the flow behavior of the colloid. To realize a smooth motion of the MF, we used a Kerosene. Kerosene is a good choice since it can dissolve the oleic acid thus helping the magnetic particles dispersion in the colloid. The fluid is the stirred and then rest for couple of hours to eliminate the water.

Then, to test the performance of the fluid a place a sample of colloid in a petri dish which is placed on top of a neodymium magnet. The dish and the magnet are separated with a working gap of 0.125 in. This setup helps in testing weather or not the fluid can form spikes under the magnetic field and also is used to test the responsiveness of the fluid when the relative position of the magnet and the petri dish is changed (see Fig. 50).

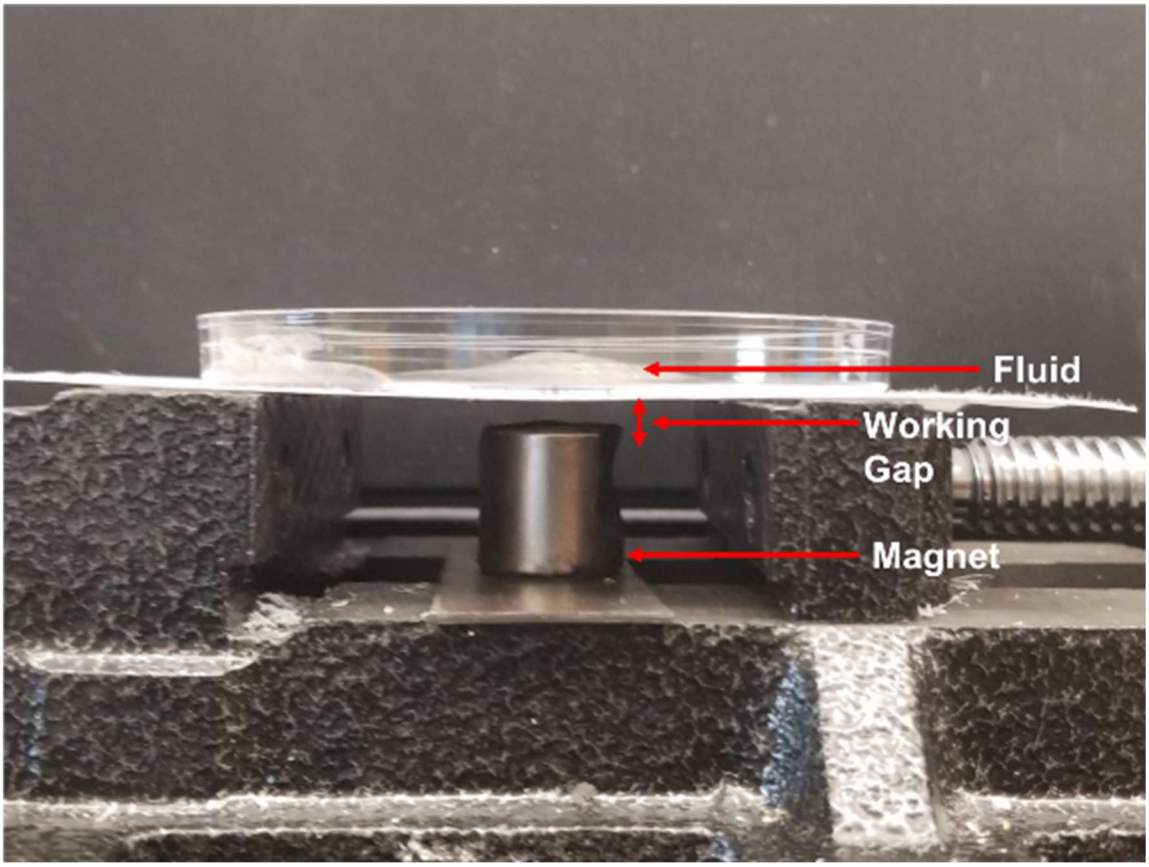

Figure 50: Photograph of a setup to test the quality of the MR fluid

5. RESULTS AND DISCUSSION[6]

In this section we are going to present and discuss the results of the experimental study conducted during this project.

5.1 Electro-Permanent Magnet and Magnetic Gradient

Electropermanent magnets can have their field switched on and off by the application of a brief electrical pulse. Electropermanent magnets have lower power consumption, less temperature rises and smaller in size compared to electromagnets, especially for the same generated magnetic field strength flux. Electropermanent magnets have been found to consume an amount of energy proportional to their volume while creating a magnetic field strength proportional to their area , which is so fundamental scaling favors their low-energy operation at small dimensions[40].

We used different frequencies of pulse with modulation signals and we observed that at a 3.3 Hz signal, the EPM generated a magnetic field gradient ranging from a maximum of .3T to a minimum of 0.08T, thus a total gradient of 0.22T. However, as the frequency increases, the total gradient value decreases. For example, at a 20Hz signal, the total observed gradient had a value 0.06T which 3.7 times smaller than the gradient at 3.3Hz. This is due to the shorter time the EPM has to switch between polarities which is

---

[6] Parts of the results and discussion are reprinted with permission from "Localized magnetic fluid finishing of freeform surfaces using electropermanent magnets and magnetic concentration" by Iskander El-Amri, Ashif Sikandar Iquebal, Arun Srinivasa, Satish Bukkapatnam, 2019. Journal of Manufacturing Processes,2018 https://doi.org/10.1016/j.jmapro.2018.05.026 , Copyright 2018 by Elsevier

not enough to fully demagnetize the residual magnetic field created in the core (see Fig. 51).

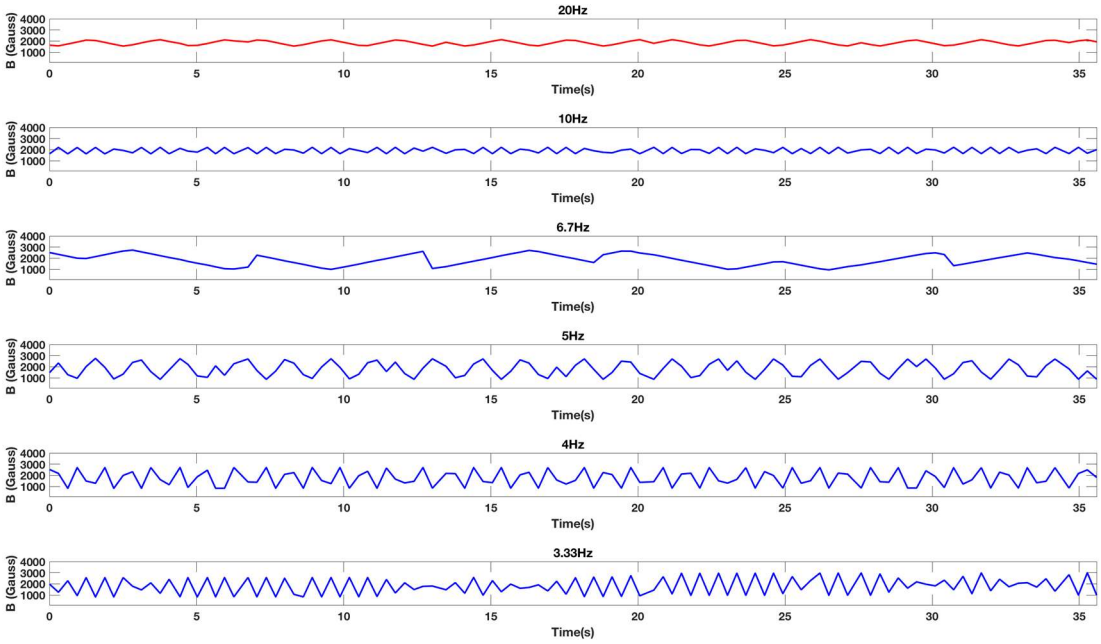

Figure 51:Magnetic field gradient with changing EPM switching frequencies

5.2 Ferrofluid Behavior

We have studied many compositions of the ferrofluid where we have varied the size of the magnetic particles as we used particles with an average size of 20 um (atomet 75) and we have also utilized nano-sized particles with size varying between 50 and 100 nm. If mixed with a carrier fluid (like mineral oil), the colloid with the smaller particles takes more time to segregate which an essential attribute for a responsive ferrofluid. Even though the smaller particles delay the precipitation due to gravity, the colloidal solution is subject to separation. Thus, using a surfactant becomes necessary to suspend the magnetic particles in the carrier fluid and also to prevent the agglomeration of said particles.

We have opted to choose oleic acid as the surfactant since it combines well with the nano size magnetite particles and also since it is relatively safe compared to other substances like tetramethylammonium hydroxide which is very toxic. Mixing the oleic acid with colloid (carrier fluid + magnetic particles) does not yield good results (separation still occurs) since oleic acid requires heat to bond with the magnetic particles.

The concentration of the oleic acid is a significant factor in the performance of the ferrofluid in response to a changing magnetic field. To verify this claim, we used three levels of oleic acid volumes to observe the responsiveness of the fluid while keeping the quantities of the magnetite (we used 10 grams of magnetite since the Nanoparticles are expensive) and kerosene fixed (43 ml of Kerosene per batch). We observed (see Table1) that at a volume of 5 ml of oleic acid, the ferrofluid had an excellent response to a changing magnetic field and also formed needle-shaped spikes. When the oleic acid volume was increased to 10 ml, the ferrofluid formed large spikes but was not very responsive to the change in magnetic field. Finally, using 15 ml, generated a fluid that formed an unresponsive bulb without any spikes. Spikes form when the magnetic force exerted on the magnetite particles overcomes the surface tension of the fluid and the gravitational pull. As the magnetic field increases, the spikes will increase in size until reaching a point where the magnetic force is too strong, and the magnetite particles precipitate towards the magnet field source [50]. Thus, spikes are a good indicator of the quality of the ferrofluid since they form when the magnetic force applied on the magnetic particles is balanced with the gravitational force applied to them and the surface tension of the carrier fluid (see Fig. 52).

After fixing all the quantities for the MRF components, we found that a ration of 5% magnetic particles, 85% carrier fluid, and 10% yields the best performance (see Table 2).

Table 1: MR fluid response vs the volume of oleic acid

Volume	**Spikes**	**Responsive motion**
5ml	+	+
10 ml	+	-
20 ml	-	-

Table 2: Quantities of MRF components

	Volume (ml or cm^3)	**Ratio**
Oleic Aid	5	0.1
Kerosene	42.51	0.85
Magnetite	2.49	0.05
Total	50	1

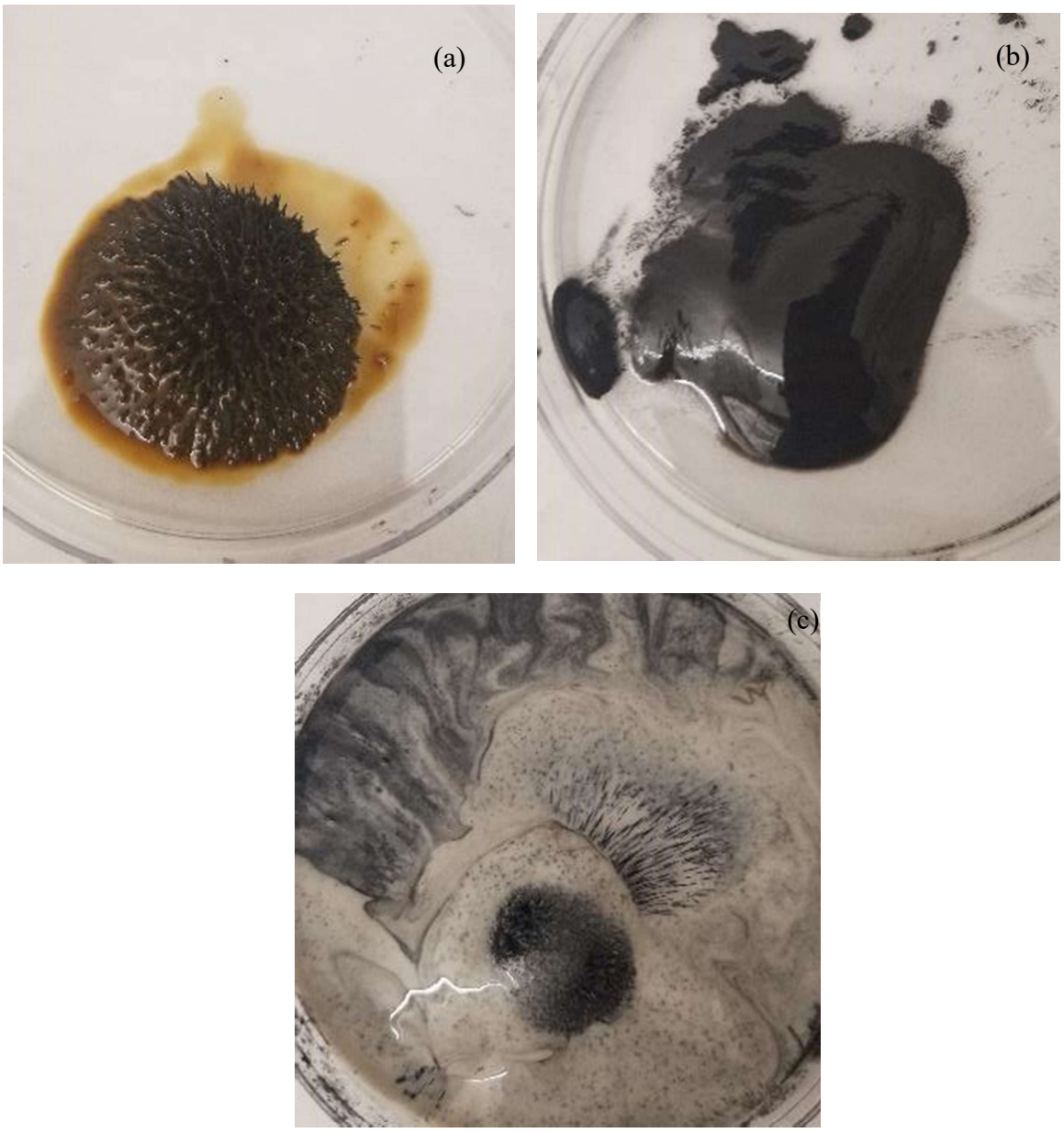

Figure 52: Photograph showing magnetic fluid response to magnetic field when different quantities of oleic acid are used (a) 5ml of oleic acid created a fluid with long spikes and quick response to changes in the magnetic field (b) 10 ml of oleic acid created a fluid with small spikes and slow response to the change in the magnetic field (c) 15 ml of oleic acid created a fluid that does not form spikes nor react to the change in the magnetic field

5.3 Using Magnetic Fluid for Polishing

5.3.1 Material Removal from Non-Flat Geometries

To demonstrate the proof of concept and the efficacy of the proposed approach in the finishing of free-form hard-to-access locations, we painted two regions of a cylindrical tube with two different permanent water-based (the paint is water soluble but water resistant when dried) acrylic paint colors (red and green) and dried the sample thoroughly [51]. Each paint layer had an average thickness of 6.5μm and covered an area of 3x1 cm2. The workpiece was placed in a beaker, and completely immersed in the specially designed MF (see Fig. 53).

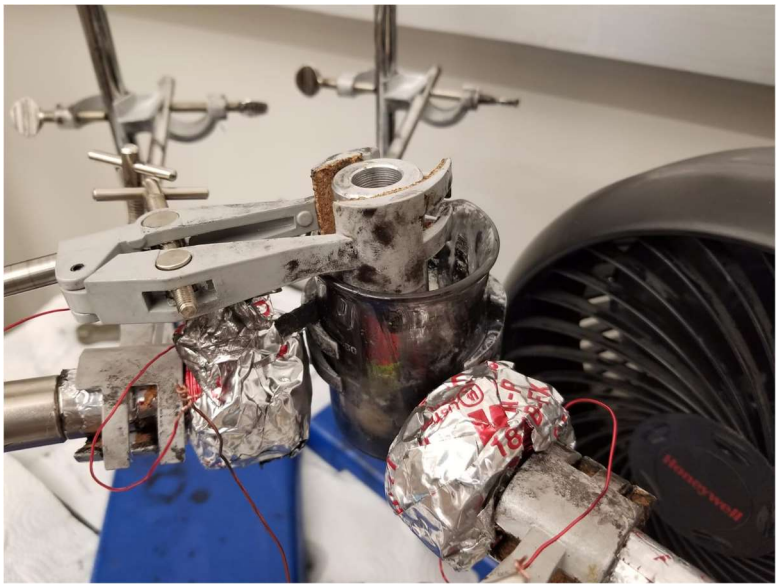

Figure 53:Experimental setup of the paint removal experiment

Through actuating the EPM, the MF over a targeted location was allowed to slosh, causing surface asperity (here, the paint) removal. We then, showed that our process was capable of removing material (in this case, acrylic paint) from a target region (green painted area with an average thickness of 6.5μm and a surface area of 3x1 cm2).

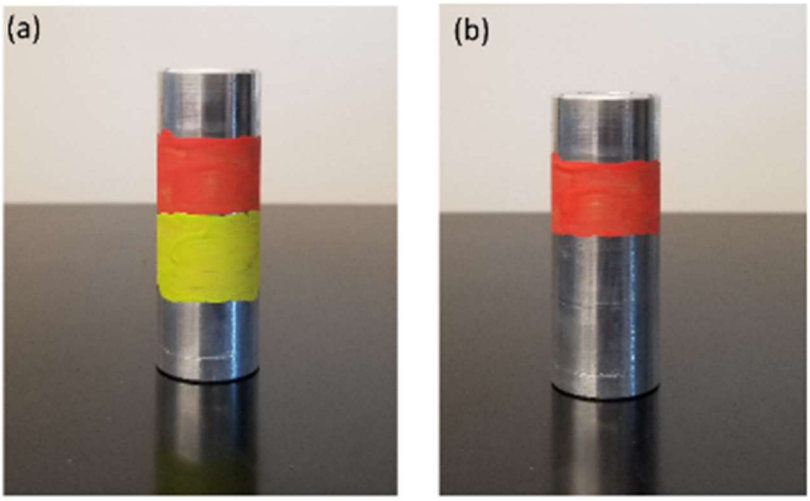

Figure 54: (a) painted cylindrical tube before polishing (b) painted cylindrical tube after polishing (Reprinted from [51])

Figure 54 (b) shows the results from experiments on localized paint removal on a high aspect ratio surface of experiments designed to show localized and selective paint removal. The workpiece was painted with two different acrylic paints, red and green, next to each other as shown in Fig. 54(a). The workpiece was polished for 90 minutes and then rinsed with distilled water. Figure 54(b) shows workpiece after polishing. It could be noted that the green paint layer was selectively removed without any changes to the red region. This demonstrates the capability of the proposed process to locally remove material from a curved surface.

5.3.2 Polishing of Polyurethane Samples

To exhibit the capability of our process to produce fine finish surfaces, we utilized a 3D printed polyurethane part as our workpiece. We have also utilized 120 grit abrasive particles in the process. The sample was secured inside the MRF container and placed in

contact with fluid. Then, a spatio-temporal magnetic gradient is created between the EPMs which forms an FMB filled with abrasive particles. The FMB is allowed to slosh back and forth against the surface of the workpiece to remove asperities and close the gaps between the infill patterns. The process is sustained for 2 hours and while the MR fluid is stirred every 5 minutes to renew the abrasive particles that separated from the FMB. After a polishing cycle (2 hours), the workpiece is cleaned with a deionized waterjet to remove MRF particles stuck on the surface, the workpiece is placed inside a container full of a water and soap mixture to separate oil residues from the surface. Finally, the workpiece is dried using a fan.

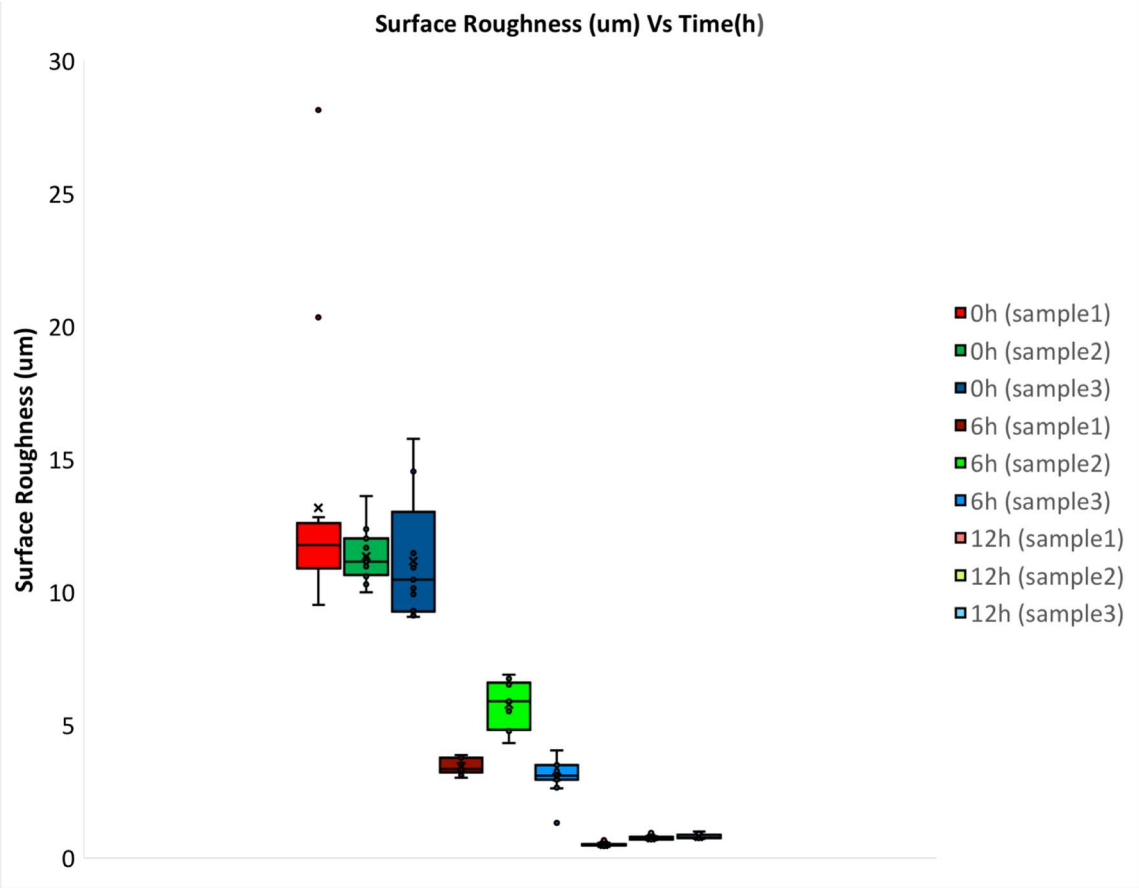

Figure 55: Evolution of Surface roughness Sa with time

The surface of the workpiece is analyzed with an optical profilometer (ZeGauge) to measure the surface roughness and check the evolution of the topology over time. The workpiece goes through 6 cycles (2 hours for polishing +1 hours for removing residue) and then the surface profile is recorded at 15 random points where each point covers an area of 800x800 um. The experiment is conducted with three different samples to ensure the repeatability of the results.

Figure 55 show a box plot to demonstrate the surface roughness evolution over time measured in surface area roughness Sa (μm) for the three samples. We observe that the initial average surface roughness (Sa) of the PLA sample is 11.91 um. The surface at this stage has a lot of defects and asperities created by FDM process. Also, due to the printing pattern, the surface has large infill gaps. These gaps measure 120um in width and 60 μm in depth on average and are also a big contributor to the un-smoothness of the workpiece surface (see Fig. 56).

After 6 hours of polishing, the average Sa dropped to 3.4558 µm and we observe that the surface features are getting flatter with a reduction of the size of the infill gaps and the planarization of the surface (see Fig. 57). After 12 hours of polishing (see Fig. 58), the Sa was in the nanometer range with an average of 700 nm. We can observe that most of the infill gaps are closing and the surface is getting flatter (see Fig. 58).

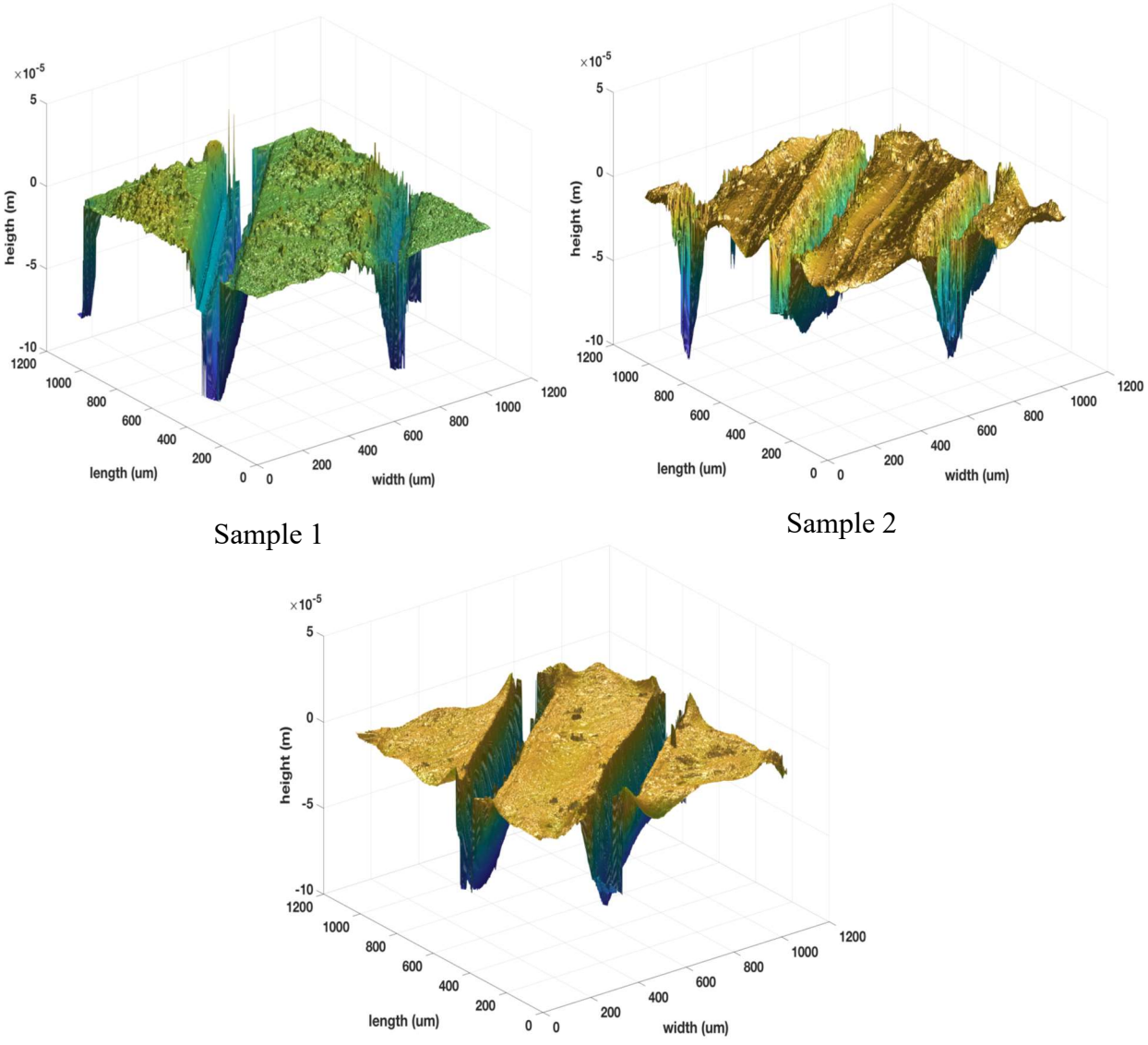

Figure 56: 3D reconstruction of the surface at the initial stage

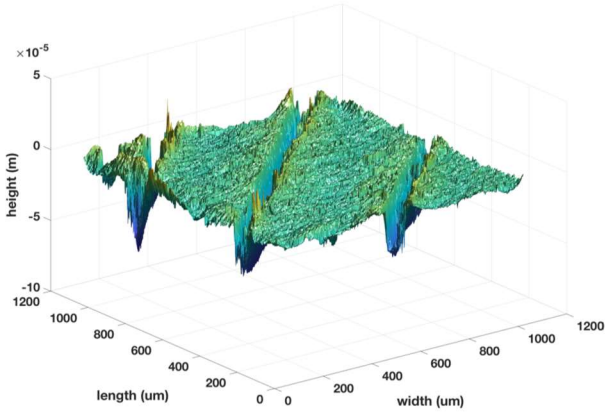

Sample 1

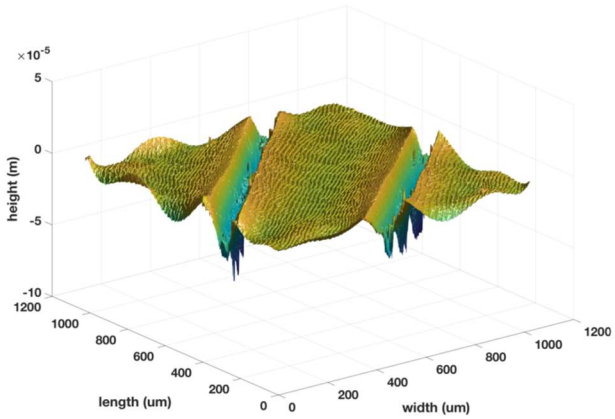

Sample 2

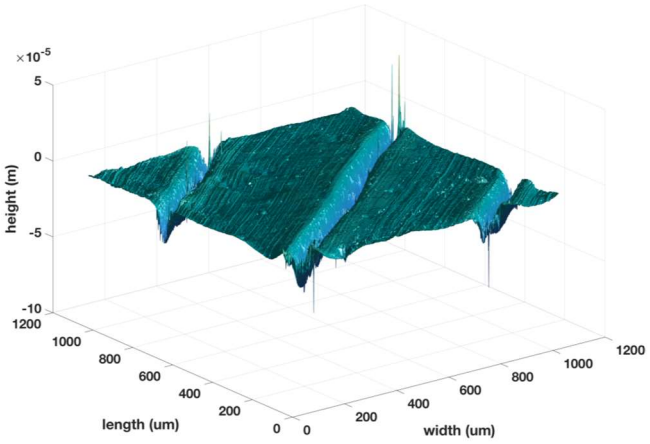

Sample 3

Figure 57: 3D reconstruction of the surface after 6h

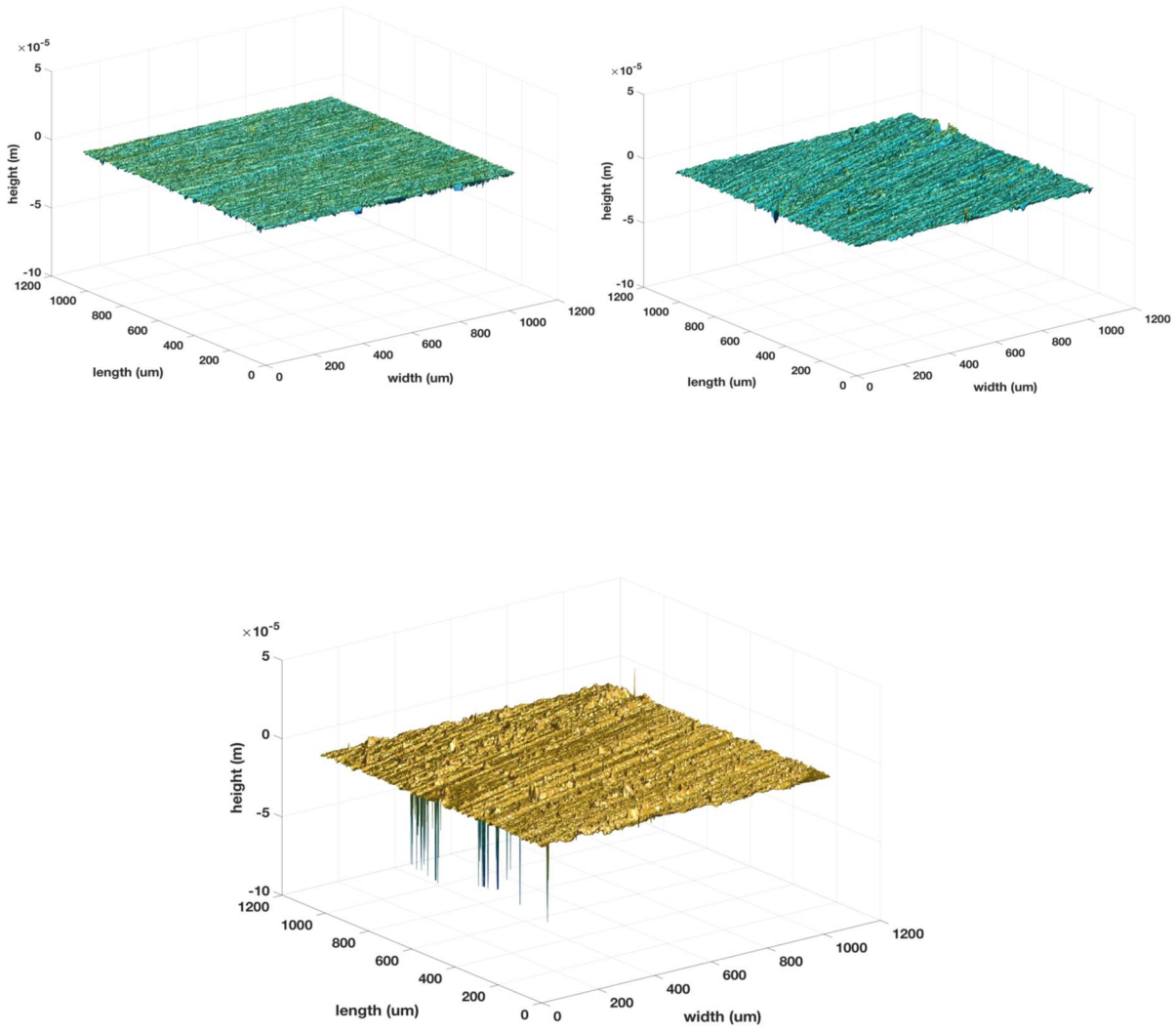

Figure 58: 3D reconstruction of the surface after 12h

The polyurethane samples have a low glass of 40°C that was measured experimentally [52] which is a concern since the EPMs release heat that propagates to the fluid container even when the cooling is active. Thus, it becomes necessary to monitor the temperature rise during the process. To investigate the matter, we placed thermocouple in the contact area between the workpiece and the magnetic fluid (see Fig. 59) and recorded the temperature rise 12 hours. We observed that the temperature rose from 25°C to 38.1°C (see Fig. 60) during the time of study thus reaching a high enough level to observe some warping in the material.

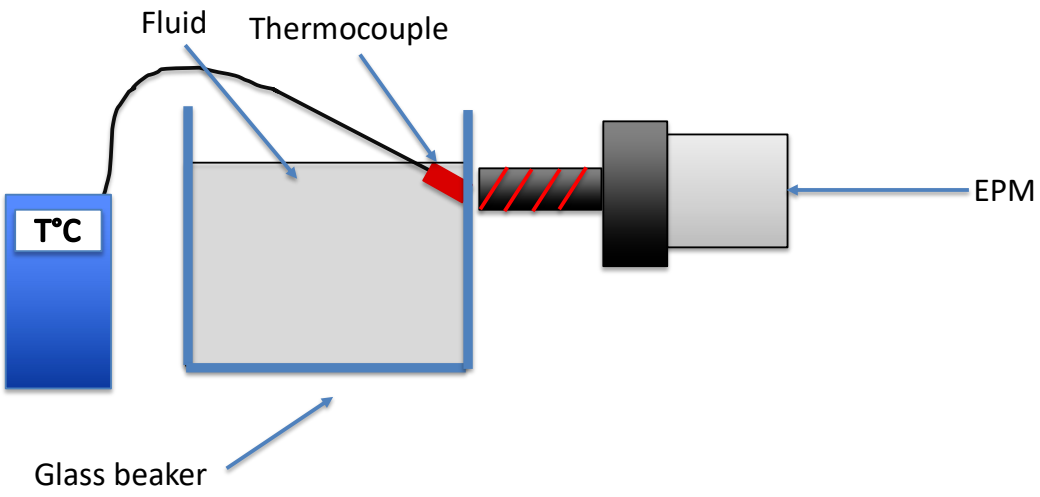

Figure 59: Schematic showing the experimental setup to measure the temperature rise inside the fluid container

We have also used the profilometer to observe the surface profile and surface roughness on the side of the polymer samples that was not subjected to polishing to assess if the surface modification is attributed to the polishing mechanism or to heat related issues. It was observed that the non-polished surface initially had an average Sa of 5.68µm

and an average Sa of 6.094µm after 12 hours of polishing (see Fig. 61 ,62,63 and 64). The Sa measurement increased slightly since the samples warped due to the heat generated by the EPMs which introduced waviness in the unpolished surfaces.

Thus, we can conclude that heat related effects are do not contribute largely to the surface modification observed in the sample side subjected to polishing, but it is due to the polishing action.

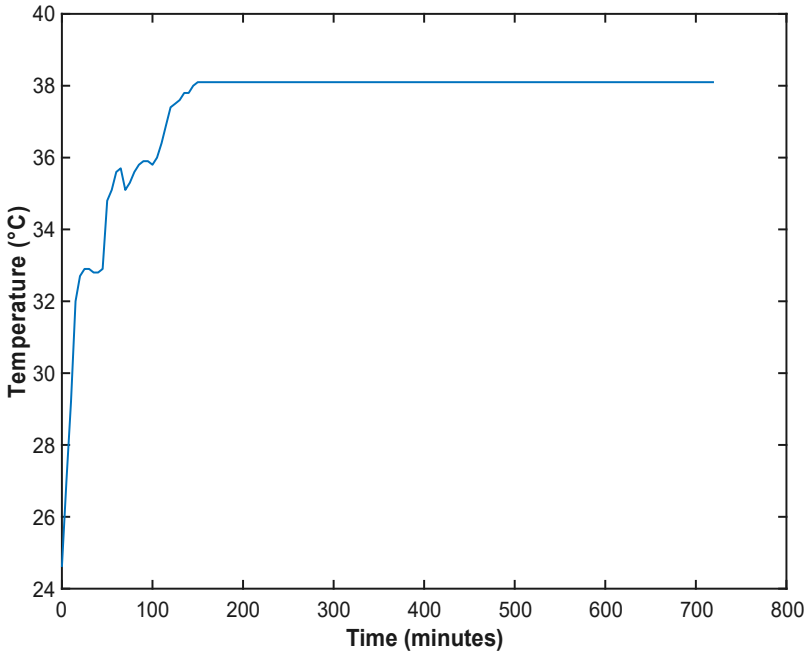

Figure 60: Temperature measured at interior side of the fluid container vs time

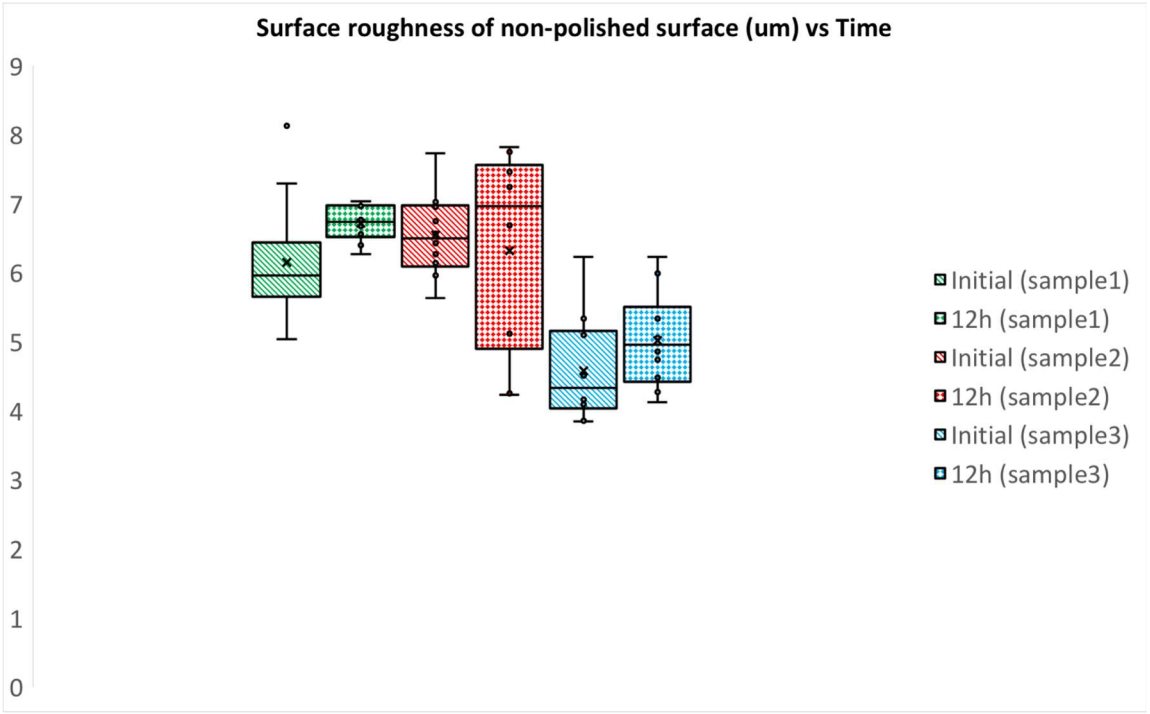

Figure 61: Surface roughness of non-polished surface vs Time

Initial

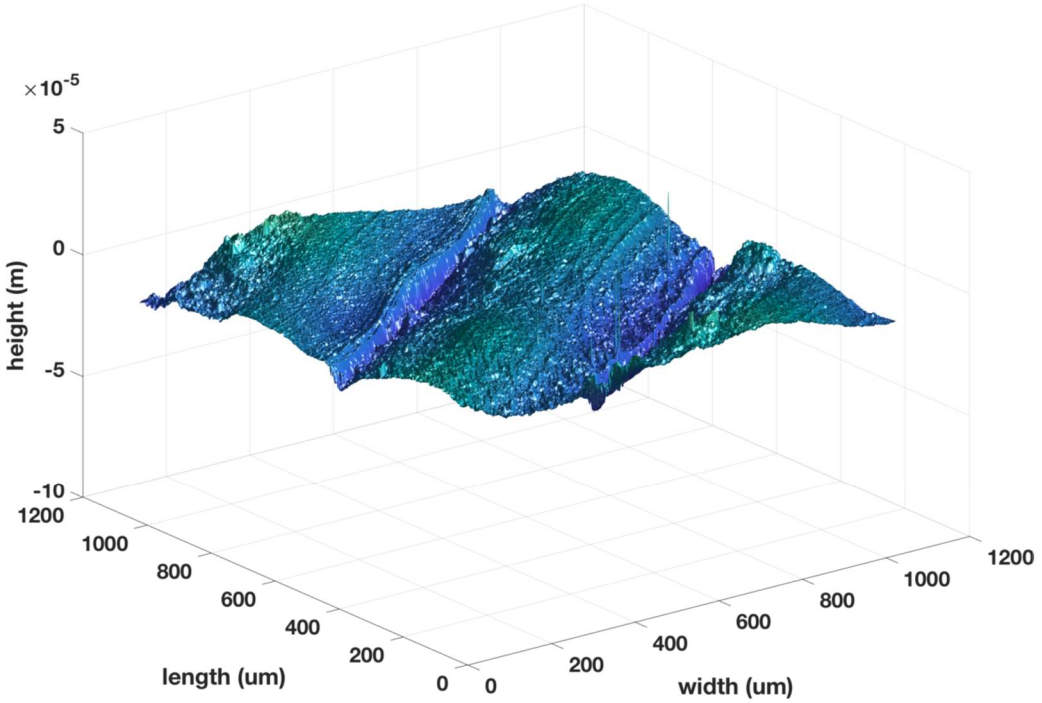

12 hours

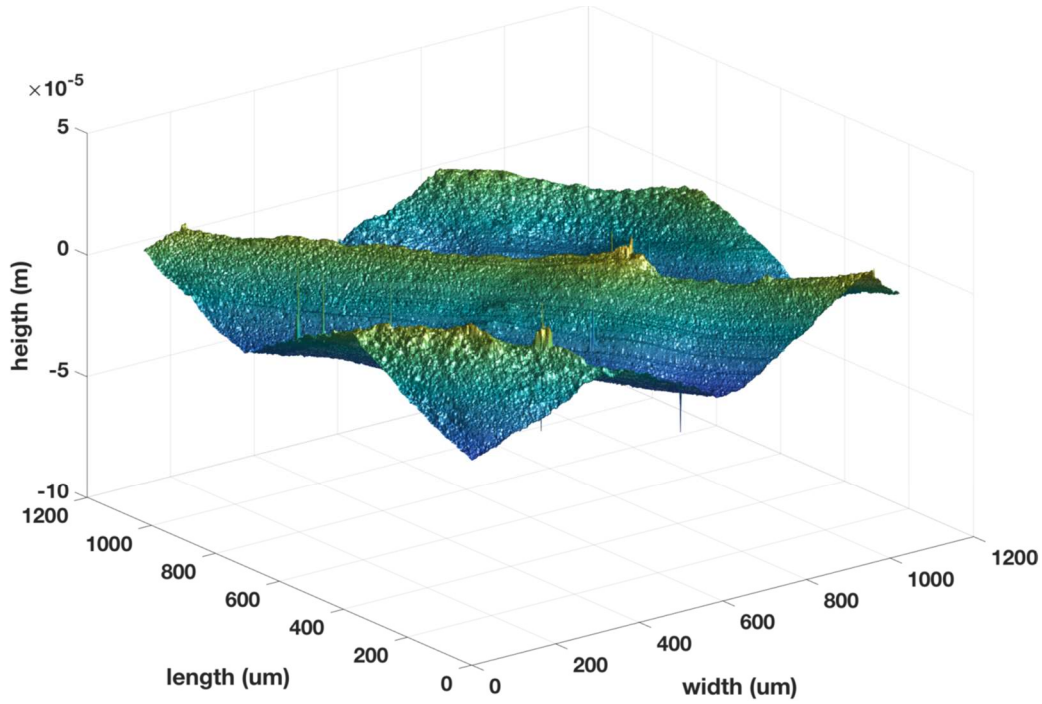

Figure 62:3D reconstruction of the surface of the unpolished side (sample1)

Initial

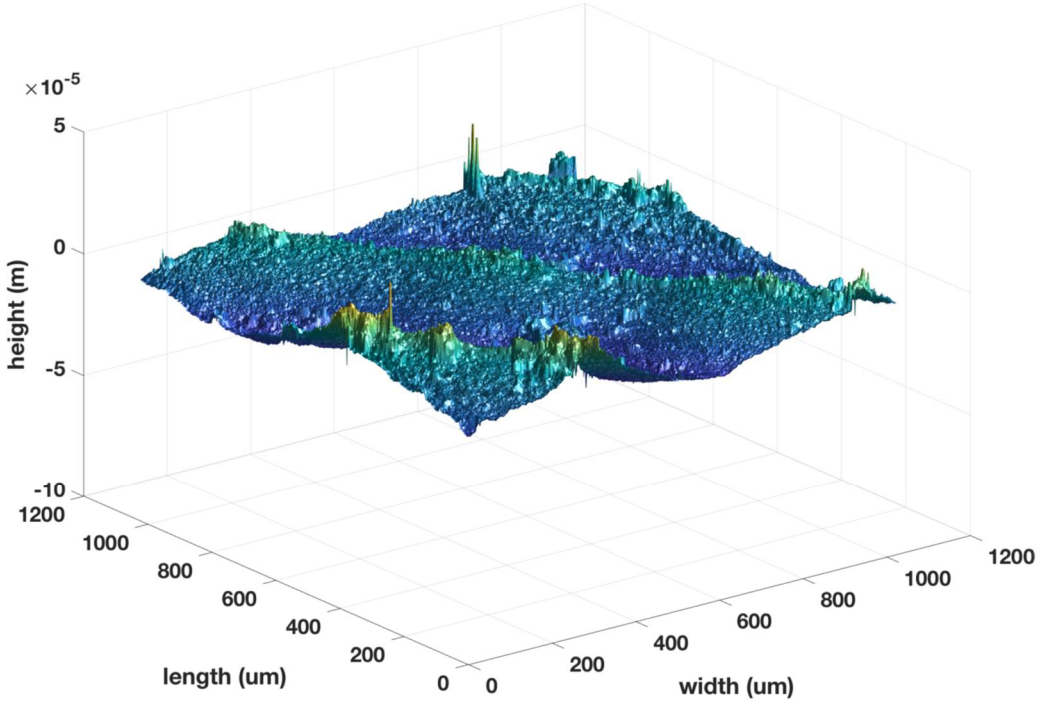

12 hours

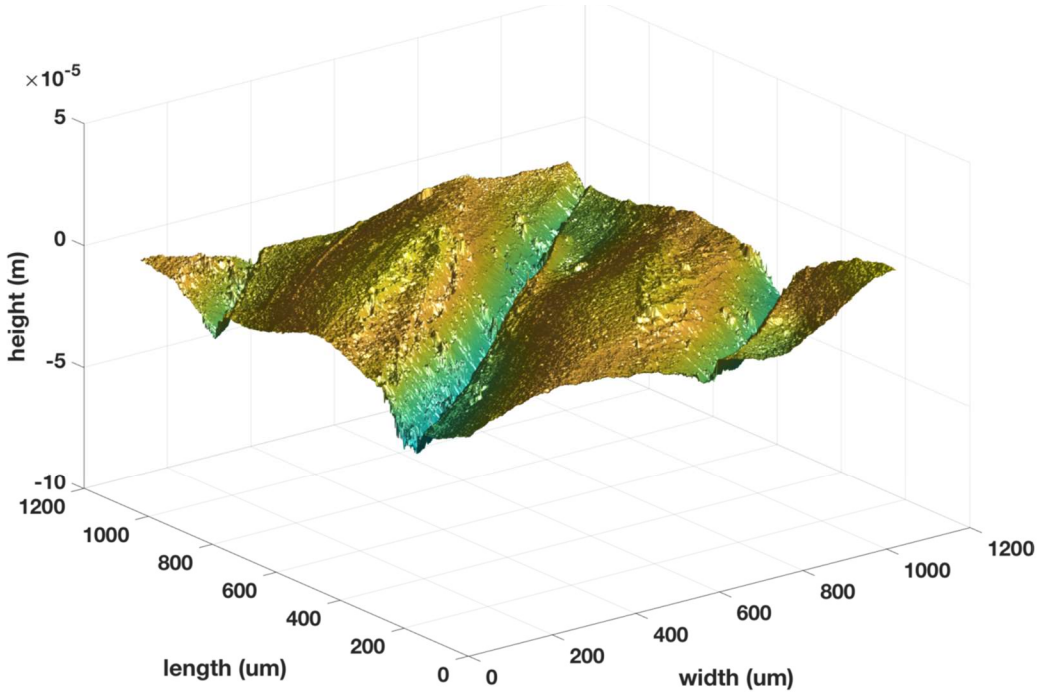

Figure 63: 3D reconstruction of the surface of the unpolished side (sample2)

Initial

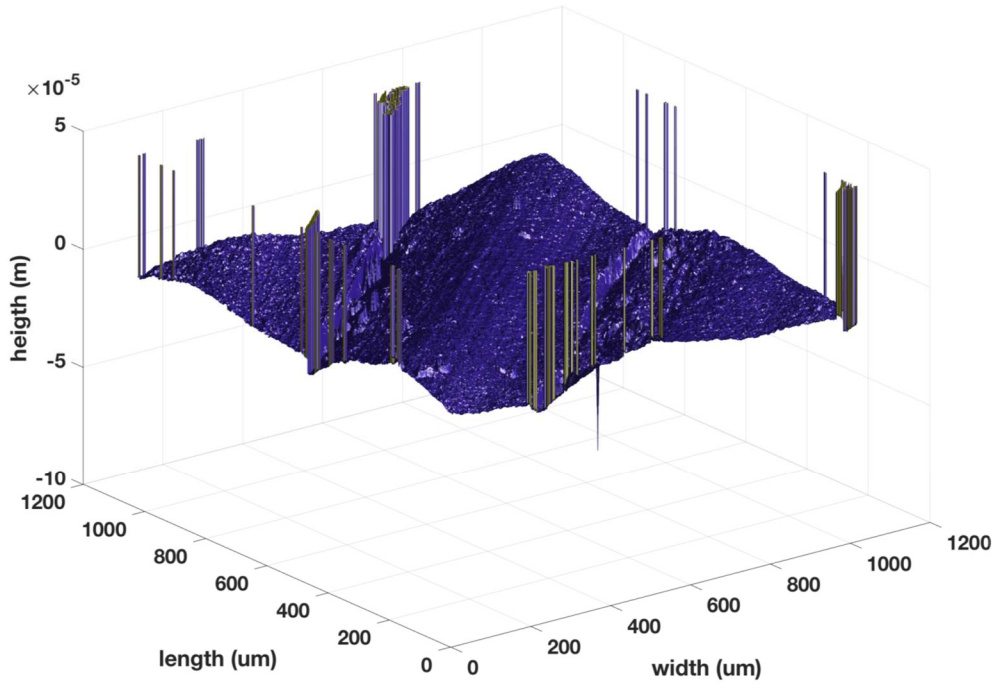

12 hours

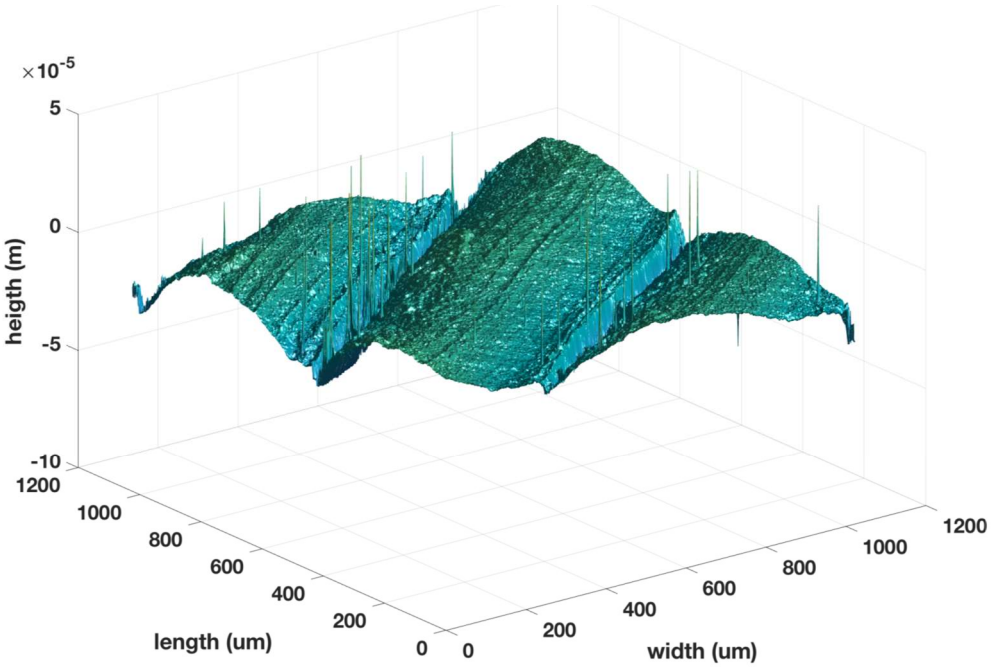

Figure 64: 3D reconstruction of the surface of the unpolished side (sample3)

6. CONCLUSIONS[7]

We have presented a novel approach for creating a spatiotemporal variation in the magnetic field by utilizing the concepts of magnetic concentration and electro-permanent magnet to polish free-form surfaces with hard-to-reach geometries using magnetic fluids. Initial experimental investigations on the localized removal of paint from a cylindrical surface present a proof of concept and also polishing some polyurethane samples from an average Sa of 11.9 μm to .69 μm. The major contribution of the present work lies in the ability to morph the magnetic fluid to the workpiece shape and create a localized sloshing action without the need to have any movable parts.

We also developed computational models to validate the efficacy and strength of magnetic concentration using the electro-permanent magnets. Computational results showed that the configuration can be used to magnify the magnetic field 3 folds at a desired location in space. In principle, by appropriately tuning the magnetic concentration setup and the magnetic fluid, it possible to modify surface properties of complex freeform geometries, especially regions inaccessible to manual or finite degree-of-freedom polishing machines.

---

[7] Parts of the conclusions are reprinted with permission from "Localized magnetic fluid finishing of freeform surfaces using electropermanent magnets and magnetic concentration" by Iskander El-Amri, Ashif Sikandar Iquebal, Arun Srinivasa, Satish Bukkapatnam, 2019. Journal of Manufacturing Processes, 2018 https://doi.org/10.1016/j.jmapro.2018.05.026, Copyright 2018 by Elsevier.

Current and future studies are focused towards finishing of additive manufactured hip and knee implants using the setup along with extending the magnetic concentration setup to include more EPMs to create specialized path plans for finishing complex geometrical surfaces and redesign their cores to increase the magnetic downforce. Further investigations are also needed to bond the abrasive particles to the magnetic fluid thus eliminating sedimentation and increasing the efficiency of the process.

REFERENCES

[1] V. K. Jain, "Nanofinishing Science and Technology: Basic and Advanced Finishing and Polishing Processes," CRC Press, 2016.

[2] Louis Columbus, "2015 Roundup Of 3D Printing Market Forecasts And Estimates," 2015. [Online]. Available: https://www.forbes.com/sites/louiscolumbus/2015/03/31/2015-roundup-of-3d-printing-market-forecasts-and-estimates/#6e79c3f81b30. [Accessed: 23-Apr-2018].

[3] A. N. Knaian, "Electropermanent magnetic connectors and actuators: devices and their application in programmable matter," Massachusetts Institute of Technology, 2010.

[4] A. D. Marchese, C. D. Onal, and D. Rus, "Soft robot actuators using energy-efficient valves controlled by electropermanent magnets," in *Intelligent Robots and Systems (IROS), 2011 IEEE/RSJ International Conference on*, 2011, pp. 756–761.

[5] F. Ochoa-Cardenas and T. J. Dodd, "Design of a Continuously Varying Electro-Permanent Magnet Adhesion Mechanism for Climbing Robots," in *Conference Towards Autonomous Robotic Systems*, 2015, pp. 192–197.

[6] T. Shinmura, K. Takazawa, and E. Hatano, "Study on magnetic-abrasive finishing. Effects of machining fluid on finishing characteristics," *Bulletin of the Japan Society of Precision Engineering*, vol. 20, no. 1, pp. 52–54, 1986.

[7] W. Kordonski and D. Golini, "Magnetorheological suspension-based high precision finishing technology (MRF)," *Journal of intelligent material systems and structures*, vol. 9, no. 8, pp. 650–654, 1998.

[8] O. Ashour, C. A. Rogers, and W. Kordonsky, "Magnetorheological fluids: materials, characterization, and devices," *Journal of intelligent material systems and structures*, vol. 7, no. 2, pp. 123–130, 1996.

[9] J. M. Ginder, L. C. Davis, and L. D. Elie, "Rheology OF MAGNETORHEOLOGICAL FLUIDS:MODELS AND MEASURMENTS," *International Journal of Modern Physics B*, vol. 10, no. 1, pp. 3293–3303, 1996.

[10] P. P. Phule, "Magnetorheological (MR) fluids: principles and applications," *Smart Materials Bulletin*, vol. 2001, no. 2, pp. 7–10, 2001.

[11] K. R. Schumacher, I. Sellien, G. S. Knoke, T. Cader, and B. A. Finlayson, "Experiment and simulation of laminar and turbulent ferrofluid pipe flow in an oscillating magnetic field," *Physical Review E*, vol. 67, no. 2, p. 26308, 2003.

[12] "Process for polishing semiconductor materials, US 3170273.pdf." 10-Jan-1963.

[13] P. Rao, S. Bukkapatnam, Z. Kong, O. Beyca, K. Case, and R. Komanduri, "Quantification of Ultraprecision Surface Morphology using an Algebraic Graph Theoretic Approach," *Procedia Manufacturing*, vol. 1, pp. 12–26, Jan. 2015.

[14] P. K. Rao *et al.*, "Process-Machine Interaction (PMI) Modeling and Monitoring of Chemical Mechanical Planarization (CMP) Process Using Wireless Vibration Sensors," *IEEE Transactions on Semiconductor Manufacturing*, vol. 27, no. 1, pp. 1–15, Feb. 2014.

[15] Z. Wang, S. T. S. Bukkapatnam, S. R. T. Kumara, Z. Kong, and Z. Katz, "Change detection in precision manufacturing processes under transient conditions," *CIRP Annals*, vol. 63, no. 1, pp. 449–452, Jan. 2014.

[16] S. T. S. Bukkapatnam, A. S. Iquebal, and S. R. T. Kumara, "Planar random graph representations of spatiotemporal surface morphology: Application to finishing of 3-D printed components," *CIRP Annals*, Apr. 2018.

[17] Michael Barrett, "Get the Most from Lubricants Through Quality Oil Analysis," 2015. [Online]. Available: https://www.pumpsandsystems.com/pumps/november-2015-get-most-lubricants-through-quality-oil-analysis. [Accessed: 14-Jul-2018].

[18] Y. Uda, T. Senga, A. Ishikawa, E. Yamamoto, T. Mitsui, and S. Hoshino, "Digital Polishing Method for CMP System using a Smaller Diameter Polishing Pad," *ASPE on 12th*, 2001.

[19] I. K. Jeong, "Chemical mechanical polishing tool, apparatus and method." Google Patents, 2005.

[20] K. Wissenbach, "Surface Treatment," in *Tailored Light 2: Laser Application Technology*, R. Poprawe, Ed. Berlin, Heidelberg: Springer Berlin Heidelberg, 2011, pp. 173–239.

[21] J. Kumstel, J. Flemmer, and A. Temmler, *Laser Polishing of Metallic Freeform Surfaces*. 2015.

[22] E. V Bordatchev, A. M. K. Hafiz, and O. R. Tutunea-Fatan, "Performance of laser polishing in finishing of metallic surfaces," *The International Journal of Advanced Manufacturing Technology*, vol. 73, no. 1, pp. 35–52, 2014.

[23] B. Rosa, P. Mognol, and J. Hascoët, “Laser polishing of additive laser manufacturing surfaces,” *Journal of Laser Applications*, vol. 27, no. S2, p. S29102, 2015.

[24] L. Zhang, J.-L. Zhuang, X.-Z. Ma, J. Tang, and Z.-W. Tian, “Microstructuring of p-Si (100) by localized electrochemical polishing using patterned agarose as a stamp,” *Electrochemistry Communications*, vol. 9, no. 10, pp. 2529–2533, 2007.

[25] J. W. Park and D. W. Lee, “Pulse electrochemical polishing for microrecesses based on a coulostatic analysis,” *The International Journal of Advanced Manufacturing Technology*, vol. 40, no. 7–8, pp. 742–748, 2009.

[26] T. Kuriyagawa, M. Saeki, and K. Syoji, “Electrorheological fluid-assisted ultra-precision polishing for small three-dimensional parts,” *Precision Engineering*, vol. 26, no. 4, pp. 370–380, 2002.

[27] D. D. Walker *et al.*, “Recent developments of Precessions polishing for larger components and free-form surfaces,” in *Proceedings of SPIE*, 2004, vol. 5523, pp. 281–289.

[28] L. Heng, Y. J. Kim, and S. D. Mun, “Review of Superfinishing by the Magnetic Abrasive Finishing Process,” *High Speed Machining*, vol. 3, no. 1, pp. 42–55, 2017.

[29] E. H. Kim, H. S. Lee, B. K. Kwak, and B. K. Kim, “Synthesis of ferrofluid with magnetic nanoparticles by sonochemical method for MRI contrast agent,” in *Journal of Magnetism and Magnetic Materials*, 2005, vol. 289, pp. 328–330.

[30] E. Auzans, D. Zins, E. Blums, and R. Massart, “Synthesis and properties of Mn-Zn ferrite ferrofluids,” *Journal of Materials Science*, vol. 34, no. 6, pp. 1253–1260, 1999.

[31] H. P. Coats, “Method of and apparatus for polishing containers.” Google Patents, 1940.

[32] T. Shinmura, K. Takazawa, E. Hatano, M. Matsunaga, and T. Matsuo, “Study on Magnetic Abrasive Finishing,” *CIRP Annals*, vol. 39, no. 1, pp. 325–328, Jan. 1990.

[33] M. Fox, K. Agrawal, T. Shinmura, and R. Komanduri, “Magnetic abrasive finishing of rollers,” *CIRP Annals-Manufacturing Technology*, vol. 43, no. 1, pp. 181–184, 1994.

[34] J.-D. Kim, Y.-H. Kang, Y.-H. Bae, and S.-W. Lee, “Development of a magnetic abrasive jet machining system for precision internal polishing of circular tubes,”

Journal of Materials Processing Technology, vol. 71, no. 3, pp. 384–393, 1997.

[35] H. Yamaguchi, T. Shinmura, and R. Ikeda, "Study of internal finishing of austenitic stainless steel capillary tubes by magnetic abrasive finishing," *Journal of Manufacturing Science and Engineering*, vol. 129, no. 5, pp. 885–892, 2007.

[36] A. M. Sidpara and V. K. Jain, "Nanofinishing of freeform surfaces of prosthetic knee joint implant," *Proceedings of the Institution of Mechanical Engineers, Part B: Journal of Engineering Manufacture*, vol. 226, no. 11, pp. 1833–1846, 2012.

[37] T. Sato, Y. B. Wu, W. M. Lin, and K. Shimada, "Study of dynamic magnetic field assisted finishing for metal mold using magnetic compound fluid (MCF)," in *Key Engineering Materials*, 2010, vol. 447, pp. 258–262.

[38] H. Guo, Y. Wu, D. Lu, M. Fujimoto, and M. Nomura, "Effects of pressure and shear stress on material removal rate in ultra-fine polishing of optical glass with magnetic compound fluid slurry," *Journal of Materials Processing Tech.*, vol. 214, pp. 2759–2769, 2014.

[39] G. E. Elias, "Lifter with electropermanent magnets provided with a safety device." Google Patents, 2000.

[40] N. A. Shirazee and A. Basak, "Electropermanent suspension system for acquiring large air-gaps to suspend loads," *IEEE Transactions on magnetics*, vol. 31, no. 6, pp. 4193–4195, 1995.

[41] C. Navau, J. Prat-Camps, and A. Sanchez, "Magnetic energy harvesting and concentration at a distance by transformation optics," *Physical review letters*, vol. 109, no. 26, p. 263903, 2012.

[42] A. J. Ward and J. B. Pendry, "Refraction and geometry in Maxwell's equations," *Journal of modern optics*, vol. 43, no. 4, pp. 773–793, 1996.

[43] K. Liu, W. Jiang, F. Sun, and S. He, "Experimental realization of strong DC magnetic enhancement with transformation optics," *Progress In Electromagnetics Research*, vol. 146, pp. 187–194, 2014.

[44] F. Sun and S. He, "Static magnetic field concentration and enhancement using magnetic materials with positive permeability," *arXiv preprint arXiv:1308.6078*, 2013.

[45] F. Gömöry, M. Solovyov, J. Šouc, C. Navau, J. Prat-Camps, and A. Sanchez, "Experimental realization of a magnetic cloak," *Science*, vol. 335, no. 6075, pp. 1466–1468, 2012.

[46] J. B. Pendry, D. Schurig, and D. R. Smith, “Controlling electromagnetic fields,” *science*, vol. 312, no. 5781, pp. 1780–1782, 2006.

[47] D. Meeker, “Finite Element Method Magnetics--Version 4.0 User’s Manual,” 2006.

[48] J. R. Brauer and IEEE Magnetics Society., *Magnetic actuators and sensors*. IEEE Press, 2006.

[49] T. Sawada, Y. Ohira, and H. Houda, “Sloshing motion of a magnetic fluid in a cylindrical container due to horizontal oscillation,” *Energy Conversion and Management*, vol. 43, no. 3, pp. 299–308, Feb. 2002.

[50] W. P. Berger, N. B. Adelman, K. J. Beckman, D. J. Campbell, A. B. Ellis, and G. C. Lisensky, “In the Laboratory Preparation and Properties of an Aqueous Ferrofluid,” *Journal of Chemical Education*, vol. 76, no. 7, 1999.

[51] S. B. Iskander El Amri , Ashif Sikandar Iquebal , Arun Srinivasaa, “Localized magnetic fluid finishing of freeform surfaces using electro-permanent magnets and magnetic concentration,” 2018.

[52] "In a personal communication with charoula kousiatza, she suggested that he polyurethane has a glass transition temperature of 40°C that she determined experimentally."

[53] Z. Yuan, Z. Jin, Y. Zhang, and Q. Wen, “Chemical Mechanical Polishing Slurries for Chemically Vapor-Deposited Diamond Films,” Journal of Manufacturing Science and Engineering, vol. 135, no. 4, p. 041006, 2013.